A Carbon Source in a Carbon Sink: Carbon Dioxide and Methane Dynamics in Open-Water Peatland Pools

Pierre Taillardat, Annika Linkhorst, Charles Deblois, Antonin Prijac, Laure Gandois, Alain Tremblay, Michelle Garneau

Global Biogeochemical Cycles

RESEARCH ARTICLE
10.1029/2023GB007909

A Carbon Source in a Carbon Sink: Carbon Dioxide and Methane Dynamics in Open-Water Peatland Pools

Pierre Taillardat[1,2], Annika Linkhorst[3], Charles P. Deblois[4], Antonin Prijac[1,5], Laure Gandois[6], Alain Tremblay[7], and Michelle Garneau[1,5]

[1]Geotop, Université du Québec à Montréal, Montréal, QC, Canada, [2]NUS Environmental Research Institute, National University of Singapore, Singapore, Singapore, [3]Department of Environmental Radioactivity and Monitoring, Federal Institute of Hydrology (BfG), Koblenz, Germany, [4]Aqua-Consult, Montréal, QC, Canada, [5]Groupe de Recherche Interuniversitaire en Limnologie (GRIL), Université du Québec à Montréal, Montréal, QC, Canada, [6]Laboratoire d'Écologie Fonctionnelle et Environnement, CNRS-UPS-INPT, Toulouse, France, [7]Hydro Québec, Montréal, QC, Canada

Abstract Peatlands store organic carbon available for decomposition and transfer to neighboring water bodies, which can ultimately generate carbon dioxide (CO_2) and methane (CH_4) emissions. The objective of this study was to clarify the biogeochemical functioning of open-water peatland pools and their influence on carbon budgets at the ecosystem and global scale. Continuously operated automated equipment and monthly manual measurements were used to describe the CO_2 and CH_4 dynamics in boreal ombrotrophic peatland pools and porewater (Québec, Canada) over the growing seasons 2019 and 2020. The peat porewater stable carbon isotope ratios ($\delta^{13}C$) for both CO_2 (median $\delta^{13}C$-CO_2: −3.8‰) and CH_4 (median $\delta^{13}C$-CH_4: −64.30‰) suggested that hydrogenotrophic methanogenesis was the predominant degradation pathway in peat. Open-water pools were supersaturated in CO_2 and CH_4 and received most of these dissolved carbon greenhouse gases (C-GHG) from peat porewater input. Throughout the growing season, higher CO_2 concentrations and fluxes in pools were measured when the water table was low—suggesting a steady release of CO_2 from deep peat porewater. Higher CH_4 ebullition and diffusion occurred in August when bottom water and peat temperatures were the highest. While this study demonstrates that peatland pools are chimneys of CO_2 and CH_4 stored in peat, it also shows that the C-GHG concentrations and flux rates in peat pools are comparable to other aquatic systems of the same size. Although peatlands are often considered uniform entities, our study highlights their biogeochemical heterogeneity, which, if considered, substantially influences their net carbon balance with the atmosphere.

Key Points:

- Peatland pools are supersaturated in CO_2 and CH_4 and represent net carbon greenhouse gas sources to the atmosphere
- CO_2 and CH_4 concentrations and fluxes fluctuated over the seasons and were explained by water table level fluctuations and temperature changes
- Net peatland carbon budgets must include open water surface emissions to avoid overestimating carbon removal from peatlands

Supporting Information:

Supporting Information may be found in the online version of this article.

Correspondence to:

P. Taillardat,
taillardat.pierre@nus.edu.sg

Citation:

Taillardat, P., Linkhorst, A., Deblois, C. P., Prijac, A., Gandois, L., Tremblay, A., & Garneau, M. (2024). A carbon source in a carbon sink: Carbon dioxide and methane dynamics in open-water peatland pools. *Global Biogeochemical Cycles*, *38*, e2023GB007909. https://doi.org/10.1029/2023GB007909

Received 6 JULY 2023
Accepted 28 MAR 2024

Author Contributions:

Conceptualization: Pierre Taillardat, Annika Linkhorst, Antonin Prijac, Laure Gandois, Michelle Garneau
Data curation: Pierre Taillardat, Annika Linkhorst
Formal analysis: Pierre Taillardat, Annika Linkhorst
Funding acquisition: Alain Tremblay, Michelle Garneau
Investigation: Pierre Taillardat, Charles P. Deblois, Antonin Prijac
Methodology: Pierre Taillardat, Charles P. Deblois
Project administration: Michelle Garneau

1. Introduction

Inland freshwater ecosystems play a central yet underappreciated role in the global carbon cycle (Regnier et al., 2022). Lakes, reservoirs, ponds, rivers, and streams receive, transport, and store terrestrial organic matter delivered through hydrological surface and subsurface processes. They also act as biogeochemical reactors, fixing atmospheric carbon dioxide (CO_2) via autotrophic activity, mineralizing terrestrial organic matter into CO_2 through heterotrophic activity (Battin et al., 2023), producing methane (CH_4) through methanogenesis, and oxidizing CH_4 to CO_2 via methanotrophy (Kumar et al., 2021; Reis et al., 2022). However, emissions are spatially and temporally variable, making estimates of their planetary contribution unclear, despite global efforts to constrain those numbers (e.g., Holgerson & Raymond, 2016; Raymond et al., 2013; Rocher-ros et al., 2023; Rosentreter et al., 2021). For example, one study described that lakes next to one another can either be a source or a sink of CO_2 depending on the land cover in their catchment (Riera et al., 1999), while other studies reported a diel amplitude in dissolved CO_2 concentrations of 21%–43% in lakes and reservoirs with greater emission rates at night when much fewer studies are conducted (Golub et al., 2023). Hydrological connectivity of a water body with its surrounding catchment also influences the carbon load it receives and its water residence time, which both affect the quantity and fate of this terrestrial-derived carbon between burial, mineralization, evasion and export (Prijac et al., 2023; Raymond et al., 2016; Sand-Jensen et al., 2022). Considering all these challenges, there is a crucial need to constrain the contribution of inland waters to the global carbon budget since they offset an important yet unclear portion of the terrestrial carbon sink (Bastviken et al., 2011; Butman et al., 2016; Raymond et al., 2013). Constraining estimates of land-atmosphere carbon exchange require an exhaustive understanding of the carbon balance of all land cover types along with their hydrological and biogeochemical interactions with one another within a defined spatial unit such as a watershed (Casas-Ruiz et al., 2023). Given that peatlands are carbon-dense and water-saturated ecosystems, small waterbodies within peatland-dominated catchments may

Resources: Alain Tremblay, Michelle Garneau
Supervision: Michelle Garneau
Visualization: Pierre Taillardat, Annika Linkhorst
Writing – original draft: Pierre Taillardat, Annika Linkhorst
Writing – review & editing: Pierre Taillardat, Annika Linkhorst, Charles P. Deblois, Antonin Prijac, Laure Gandois, Michelle Garneau

receive and release large quantities of dissolved and particulate organic carbon as well as dissolved C-GHGs. As such, peatland open-water pools may even need to be considered as specific water body categories to refine global scale estimates, as suggested in previous syntheses (e.g., Holgerson & Raymond, 2016; Rosentreter et al., 2021).

Open-water pools, or ponds, are distinct peatland microforms (i.e., small-scale land covers) that contribute to the spatial hydrological and ecological heterogeneity of northern peatland ecosystems (Harris et al., 2019). The existence of peatland pools has been subject to various hypotheses (Belyea & Lancaster, 2002; Comas et al., 2011; Foster et al., 1983; Garneau et al., 2018), which may all be correct but vary between regions. Regardless of their origins, peatland pools are likely to play central biological and ecological roles and deserve full attention. According to the Boreal-Arctic Wetland and Lake Dataset (BAWLD), peatland pools occupy 260,000 km^2, which is equivalent to 6% of the northern peatland area (Olefeldt et al., 2021) and within the same order of magnitude as what reservoirs cover globally (Raymond et al., 2013). Nevertheless, the biogeochemical processes driving carbon and C-GHG dynamics to and within the pools have not been fully described. Additionally, C-GHG from pools have not been clearly assessed within peatland budgets at the catchment scale, which prevents understanding their importance in the net ecosystem carbon balance.

Within open-water peatland pools, hydrological mechanisms and biogeochemical processes can influence the production, transformation and loss of organic and inorganic carbon. Just like any freshwater system, particulate and dissolved carbon in peatland pools can either originate from allochthonous input or in situ metabolism (i.e., the balance of the metabolic fluxes, gross primary production (GPP) and ecosystem respiration (ER; autotrophic and heterotrophic), which is equivalent to net ecosystem production (NEP = GPP − ER)). Considering that open-water pools are surrounded by peat, an important fraction of the carbon present in the pools is introduced through diffusion and advection from peat porewater. For instance, Prijac et al. (2022) demonstrated that most of the dissolved organic carbon (DOC) in the pools originated from peat vegetation rather than autotrophic bacterial activity. Yet, Prijac et al. (2022) also reported an important difference in concentrations, optical properties, molecular composition, and stable isotopic values, which suggest that DOC degradation processes are happening either at the peat porewater-pool interfaces or within the pools, just like observed elsewhere for boreal streams draining boreal landscapes, including peatlands (Rasilo et al., 2017). DOC can be degraded and converted to CO_2 as a result of photochemical oxidation, an abiotic reaction that breaks down and oxidizes organic compounds through solar radiation (Granéli et al., 1998), or as a result of in situ heterotrophic bacterial degradation. Methane in peatland pools is expected to be released from peat porewater via diffusion or ebullition (Dean et al., 2023; McEnroe et al., 2009). Additionally, a fraction of the diffused methane can be oxidized in the peatland water and converted into CO_2 via methanotrophic microbial activity present under oxic conditions (Hanson & Hanson, 1996; Reis et al., 2022) and, to a smaller extent, anoxic conditions (Schubert et al., 2011; Sivan et al., 2011). The variety of biogeochemical processes and interconnectivity between them complicate the identification of each pathway. However, the use of stable carbon isotope ratios ($\delta^{13}C$) along with elemental analysis and continuous in situ measurements can help develop interpretations to better understand freshwater carbon cycling (e.g., Campeau et al., 2018; Rocher-Ros et al., 2021; Taillardat et al., 2022), including in peatland ecosystems.

This study aims to describe the biogeochemical functioning of open-water peatland pools and assess their importance in carbon budgets. More specifically, we wanted to test the hypothesis that pools are primarily fueled by peat-derived porewater seepage and that they emit and export large amounts of CO_2 and CH_4. This study was designed to address the following three research objectives: (a) identify the biogeochemical processes that explain CO_2 and CH_4 concentrations in and emissions from open-water peatland pools; (b) synthesize and compare the C-GHG concentrations in and emissions from open-water peatland pools with other aquatic systems; (c) assess the importance of open-water pools in the peatland carbon budget at the ecosystem scale. In link with the research objectives, we wanted to test the following three hypotheses: (a) the dissolved carbon in the pools predominantly originates from peat organic matter rather than in situ autotrophic microbial productivity; (b) peatland pools are a unique biogeochemical freshwater category because of the surrounding carbon-dense peatland they drain; and (c) C-GHG emissions from pools offset a substantial fraction of the peatland ecosystem carbon sink function.

2. Methods

2.1. Study Site

The study was conducted in a 2.22 km^2 peatland-dominated catchment (Figure 1b; 50°31′N, 63°12′W; elevation: 108 ± 5 m above sea level) within the La Romaine Watershed (Québec, Canada) located in the bioclimatic

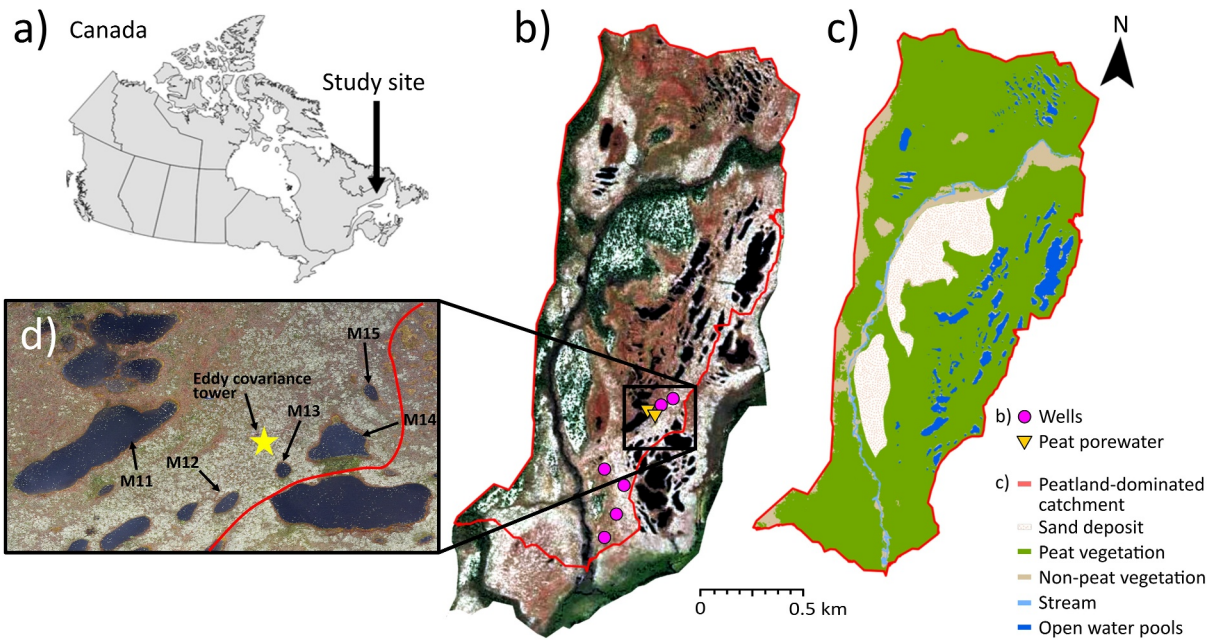

Figure 1. (a) Location of the study area in Eastern Canada; (b) aerial photograph image from « World Imagery ArcGIS » from 8 May 2017; (c) land cover representation of the peatland-dominated catchment study site; and (d) aerial photograph zoom from a drone image to show the five studied pools (M11 to M15).

spruce-moss domain of the closed boreal forest of Eastern Canada (Payette et al., 2001). The delineation of the peatland drainage catchment was made using a LiDAR (Light Detection and Ranging) image from 17 August 2004 (source: Hydro-Québec) by computing a digital elevation model using the 3D analyst tool in ArcGIS v10.5.1 (Environmental Systems Research Institute, USA). The terrestrial and aquatic surfaces within this catchment were measured using a remote sensing image from « World Imagery ArcGIS » from 8 May 2017 with a resolution of 0.3 m. The ombrotrophic peatland vegetation and open-water pools cover 82.4% of the catchment surface; the other land covers are exposed bedrock with lying sand deposits (10.4%), non-peat vegetation (7.19%), and a headwater stream draining the catchment (0.5%). The total peatland area is 2.60 km^2, but only 1.82 km^2 is located within the studied catchment (Figure 1b). Peat started to accumulate 9,070 calibrated years before the present, following the postglacial Goldthwait Sea retreat, and today, the maximum peat depth reaches 440 cm (Primeau & Garneau, 2021). The regional 30-year (1990–2019) normal mean annual temperature, rainfall, and snowfall are 1.5°C, 422 mm, and 589 mm, respectively (Environment Canada, 2023). The coldest and warmest months are January and July, with mean daily temperatures of −13.9°C and 15.1°C, respectively. Average monthly temperatures above 0°C occur from May to October.

The peatland has a patterned surface of alternating microforms characterized by hummocks, lawns, hollows, and pools. Pools occupy 108,112 m^2, representing 4.9% of the studied catchment and 5.8% of the peatland surface within the catchment. In total, 164 pools >10 m^2 were identified in the catchment. The median and mean pool sizes were 109 and 659 m^2, respectively. The 25 largest pools (15% of the total number of pools) represented 80% of the total pool area, while the 118 smallest pools (72% of the total number of pools) only represented 10% of the total pool area. Research documenting C-GHG dynamics in the draining stream and dissolved organic matter (DOM) composition and exchange along the peat-pool interface within this study site has previously been published (Prijac et al., 2022, 2023; Taillardat et al., 2022).

Instrument data and manual samples were collected from five pools within the peatland during the growing seasons of 2019 and 2020. These five pools were selected based on their size. First, we mapped all pools >10 m^2 located within the peatland and binned them into five groups based on their surface area and population (Table S1 in Supporting Information S1). Second, for each group, the pool closest to the eddy covariance system was selected for further analyses (Figure 1d). The pools' respective surface areas were determined via ArcGIS Pro 2.8.0, and their depths were manually measured on-site using a meter stick at multiple locations within the pool and averaged (Table S2 in Supporting Information S1).

2.2. Manual Measurements

Data via manual sampling were collected monthly during the snow-free season in 2019 from June to October. This resulted in a total of five field campaigns in each of which all five pools were sampled within the same day.

2.2.1. Water Samples

Partial pressure (pCO_2 and pCH_4) and stable carbon isotope values ($\delta^{13}C\text{-}CO_2$ and $\delta^{13}C\text{-}CH_4$) were determined using the headspace technique (see Taillardat et al. (2022) for a complete description). On each sampling day, triplicate samples were taken at each sampling point between 09:00 and 16:00. Additionally, samples were collected within each of the five studied pools every 2 hr over a 24-hr sampling effort on 4–5 August 2019. Samples were analyzed in the laboratory using a cavity ring-down spectroscopy (CRDS) C-GHG analyzer (G2201-i, Picarro Inc., USA) equipped with a gas autosampler (SAM, OpenAutosampler Inc., Canada). The stable isotopic ratio for CO_2 and CH_4 data are reported in standard data notation (δ) expressed in ‰ relative to the Vienna Pee Dee Belemnite standard. To ensure consistency of the measurements, gas standards (AlphagazTM Isotope Natural Air, Airgas, USA) were analyzed at the beginning, in the middle (after 25 samples), and at the end of each run.

Peat porewater samples were collected during the field campaigns in June, August, and September 2019 using a peristaltic pump and tubing fixed to a 1-m metallic rod which was directly inserted into the peat. Two microforms (a hummock and a hollow) were selected to account for spatial variation, and samples were taken 30 cm, 70 cm, and 100 cm below the peat surface in each microform. Subsurface water samples from the wells (i.e., 2-m PVC (Polyvinyl Chloride) pipes inserted into the peat) were collected using a peristaltic pump after flushing the first liter of water. Water samples for dissolved CO_2 and CH_4, $\delta^{13}C\text{-}CO_2$, and $\delta^{13}C\text{-}CH_4$ estimates were collected from two porewater sampling sites and six wells in triplicate (Figure 1b). Dissolved oxygen (DO) concentration, pH, and temperature were measured in these pore- and well-water samples using a multiparameter probe (WTW Multi 3620 IDS, Xylem Analytics, Germany).

Temperature, DO, pH, and specific conductivity in the pool water were measured using the above-mentioned multiparameter probe whenever dissolved gas samples were collected. Samples for DOC concentration analysis were filtered using pre-burned 0.7-µm GF/F filters (Whatman, USA), acidified to pH 2 using 1-M HCl and stored in 40-mL glass vials. Analyses were performed using the catalytic oxidation method followed by non-dispersive infrared (NDIR) detection of produced CO_2 (total organic carbon (TOC) analyzer TOC-L, Shimadzu, Japan) with a quantification limit of 0.1 mg C L^{-1}. Certified materials (ion 915 and ion 96.4, Environment and Climate Change Canada, Canada) were included in the analytical loop, and the recovery was >95% of the certified value. To account for the total dissolved carbon ($DOC + CO_2 + CH_4 + HCO_3^-$), we also calculated the bicarbonate (HCO_3^-) concentration using dissolved CO_2 and pH via the program CO_2SYS (Lewis et al., 1998) with the carbonate dissociation constants K_1 and K_2 taken from Millero et al. (2006) and the $KHSO_4$ from Dickson (1990).

2.2.2. Diffusive CO_2 and CH_4 flux

Water-atmosphere CO_2 and CH_4 fluxes (FCO_2 and FCH_4) were measured using a CRDS mobile gas concentration analyzer (Picarro GasScouter™ G4301, USA) during data collection in 2019 using the floating chamber method (Frankignoulle et al., 1998). A custom-built dynamic floating chamber (0.157 m^2, 0.042 m^3) was connected to the CRDS C-GHG analyzer in a closed loop. A temperature sensor (HOBO Pendant UA-002-08 Temperature/Light, ONSET, USA) was installed in the chamber headspace to measure the temperature every ten seconds. Each flux measurement of each sampling point was conducted over five incubation periods of five minutes each, and calculated following Equation 1.

$$F = S_{pCO_2} \text{ OR } S_{pCH_4} \cdot \frac{V}{R \cdot T_{\text{chamber air}} \cdot A} \quad (1)$$

where F is the water-air CO_2 or CH_4 flux (mmol m^{-2} s^{-1}); S_{pCO_2} or S_{pCH_4} is the slope of the CO_2 or CH_4 concentration inside the chamber over time (ppmV s^{-1}); V is the total volume of the flux chamber + tubing (m^3); R is the ideal gas constant (atm m^3 K^{-1} mol^{-1}); $T_{\text{chamber air}}$ is the absolute air temperature in the chamber (K); and A is

the water surface covered by the chamber (m^2). The slopes were calculated using linear regressions. Only regressions with an $R^2 \geq 0.89$ were used to calculate F.

2.2.3. Gas Transfer Velocity Determination

The gas transfer velocities (k; m d^{-1}) of CO_2 and CH_4 were derived using Equation 2:

$$k = \frac{F \cdot 3.6}{\left(K_0 \left(p_{\text{water}} - p_{\text{air}}\right)\right)} \quad (2)$$

where F is the flux measured with the floating chamber expressed in mmol m^{-2} s^{-1} (Equation 2), K_0 is the solubility coefficient expressed in mol L^{-1} atm^{-1} (Weiss, 1974), and p_{water} and p_{air} are the gas partial pressures in water and air, respectively, expressed in µatm.

Based on field measurements during the campaigns of June, August, and September 2019, k was determined for each sampling point ($n = 5$), combining direct flux chamber measurements and dissolved CO_2 and CH_4 using the headspace technique (see Section 2.2.1). For sampling periods in which only dissolved CO_2 and CH_4 samples were collected (i.e., no aquatic flux chambers), the median values specific to each sampling point were used.

The k values were normalized to k_{600} values, which represent k at 20°C in freshwater at a Schmidt number of 600 as calculated according to Equation 3:

$$k_{600} = k \cdot (S_c/600)^n \quad (3)$$

where S_c is the Schmidt number of a gas at a given temperature (Wanninkhof, 1992). We used $n = 0.5$ for a wind speed >3 m s^{-1} (Goldenfum, 2011).

2.2.4. Ebullitive CH_4 Flux

The CH_4 flux via ebullition (i.e., bubbling) was estimated from a total of 16 bubble traps (i.e., inverted funnels, 30 cm diameter, 0.07 m^2 area) in the summer of 2019. Eleven bubble traps were deployed from 14 June to 7 August 2019 and five more from 7 August to 7 September 2019, and emptied and analyzed once at the end. The bubble traps were floating underneath the water surface in three different pools. They were entirely submerged in water with their wide-open ends directed toward the bottom of the water body and their narrow ends facing upwards. At their upward-facing narrow ends, the bubble traps were sealed with rubber caps. As gas entered the bubble traps, water was displaced and gas accumulated underneath the rubber caps. The trapped gas was collected through the rubber caps using a 60-mL polyethylene syringe equipped with a needle. The total gas volume was read from the syringe scale. All gas samples were stored in pre-evacuated 12-mL glass exetainers (Labco International Inc., UK) for later estimation of CO_2 and CH_4 concentrations and $\delta^{13}C\text{-}CO_2$ and $\delta^{13}C\text{-}CH_4$. The number sampling frequency and spatiotemporal distribution of the deployed traps do not allow a detailed analysis of the spatiotemporal variability of ebullition flux from the pools. We therefore solely used the average ebullitive flux estimated from the 16 bubble trap deployments for a rough estimate of total ebullitive flux from the pools for inclusion in the overall carbon budget of the peatland.

2.3. Automated Measurements

From 25 June 2020 to 27 August 2020, an automated C-GHG monitoring system was installed in pool M11 (see Figure 1) to measure pCO_2 and pCH_4 in water every three hours starting at midnight. Equipment and setup are described in Deblois et al. (2023) and were similar to those used in Taillardat et al. (2022). Briefly, water was sampled at a water depth of 10 cm using a peristaltic pump and channeled into a gas equilibrator (Minimodule membrane contactors, Liqui-Cel, USA) for 30 min to allow equilibration of partial pressure between water and air phase in the module lumen. pCO_2 was measured with a non-dispersive infrared sensor (Li-Cor Li-850, USA; 0–20000 ppm; 2%–4% accuracy), and pCH_4 with a Tunable Diode Laser Spectroscopy sensor (TDLS; Axetris LGD Compact A, Switzerland; 0–1000 ppm, precision ≤0.8 ppm). Data were recorded by a data logger (CR1000x, Campbell Scientific, USA) at the end of each measuring cycle for a total of eight measurements per day (i.e., every three hours). Partial pressures (ppm) were converted to concentrations (µM) based on water temperature

and gas solubility coefficient from Weiss (1974) for CO_2 and from Lide (2007) for CH_4, as described in Goldenfum (2011).

A micrometeorological station that included an eddy covariance system with a sonic anemometer (CSAT3, Campbell Scientific, USA) and InfraRed Gas Analyzers (IRGAs) for quantification of the CO_2 & H_20, and CH_4 flux (LI-7200 and LI-770, LI-COR Biosciences, USA) was installed about 600 m NW of the outlet (Figure 1b). Additionally, we measured the peat water table depth using a water level pressure sensor (U20 Hobo, ONSET, USA) in a PVC pipe inserted in a 2-m deep well into the peat. The barometric pressure was subtracted from the ambient atmospheric pressure using a second pressure sensor left aboveground.

2.4. Systematic Literature Review

A systematic literature review was conducted to provide a synthesis of dissolved CO_2 and CH_4 concentrations and fluxes from open-water peatland pools globally. A literature search through the Scopus database was conducted using the search string "(pool OR pond) AND (carbon OR CO_2 OR CH_4 OR methane) AND (peatland OR wetland OR bog OR fen)" on 3 October 2023. A total of 1,892 documents were captured. A title screening was conducted to only download papers that appeared relevant to our study (e.g., the term "pool" was often used to describe the carbon stocks in peatlands ("carbon pool") and not about a water body), which narrowed down the number of relevant papers to 92. The selected papers were then downloaded, and data were extracted when possible or relevant. One key consideration was to exclude papers that referred to thermokarst since they represent a distinct aquatic system. The database constructed from the literature review is based on 38 independent studies and 284 individual study sites (Supporting Information S2).

2.5. Data Processing and Statistical Analysis

All data processing was done using R version 4.0.2 (Core Team R, 2021). To quantify and express the seasonal amplitude of daily CO_2 and CH_4 variation, we used the same data treatment as in Taillardat et al. (2022).

3. Results

3.1. Dissolved Carbon Composition in the Peat Porewater

A median dissolved carbon concentration of 51.1 mg C L^{-1} (mean: 47.2 mg C L^{-1}; range: 6.3–93.5 mg C L^{-1}) was measured in peat porewater, with 27.2 mg C L^{-1} or 53% present as dissolved CO_2, 20.2 mg C L^{-1} or 40% present as DOC, 3.2 mg C L^{-1} or 6% present as dissolved CH_4, and the remaining as 0.4 mg C L^{-1} or 1% as HCO_3^- (Table S2 in Supporting Information S1). The lowest $\delta^{13}C$ values in peat porewater were for $\delta^{13}C$-CH_4, which ranged from −82.4‰ to −68.5‰. The second lowest was $\delta^{13}C$-DOC (−28.3‰ to −25.0‰), and the highest was $\delta^{13}C$-CO_2 (−9.9‰ to −0.2‰).

3.2. Variability of CO_2 and CH_4 Dynamics From Discrete Measurements

The surface water of all five pools M11–M15 determined from discrete measurements in June to September 2019 was supersaturated in CO_2 and CH_4 relative to the atmosphere. Median dissolved carbon concentrations in the surface water were 13.3 mg C L^{-1} (range: 3–28.6 mg C L^{-1}). Despite these supersaturated conditions, CO_2 and CH_4 concentrations represented only 3.7% and 0.1% of the total dissolved carbon in pools, respectively. The bulk of dissolved carbon was present in its organic form as DOC (median: 12.8 mg C L^{-1}; range: 3.0–26.7 mg C L^{-1}), while HCO_3^- was insignificant (median: 6.0 µg C L^{-1}; range: 3.6–32.4 µg C L^{-1}; Table S2 in Supporting Information S1). Peat porewater was more concentrated in CO_2 and CH_4 than the pool water (55 and 159 times for CO_2 and CH_4, respectively), while the DOC content was within the same order of magnitude for the two environments (median peat porewater DOC concentration: 20.2 mg C L^{-1}; Table S2 in Supporting Information S1). The median $\delta^{13}C$-CO_2 was higher in the peat porewater (−3.8‰) than in the pool water (−12.4‰), whereas the median $\delta^{13}C$-CH_4 was lower in the peat porewater (−77.2‰) than in the pool water (−66.2‰; Table S2 in Supporting Information S1).

The overall median diffusive CO_2 and CH_4 fluxes in the five pools were 220.0 mg C m^{-2} d^{-1} (110.0–940.0 mg C-CO_2 m^{-2} d^{-1}) and 17.7 mg C-CH_4 m^{-2} d^{-1} (3.0–447.9 mg C-CH_4 m^{-2} d^{-1}). Leaving aside pool M11, a negative relationship between pool size, dissolved gas concentrations (Figures 2e and 2f) and fluxes was observed (Figures 2a and 2b). The highest CO_2 and CH_4 concentrations and CO_2 fluxes were found in the smallest pool

10.1029/2023GB007909

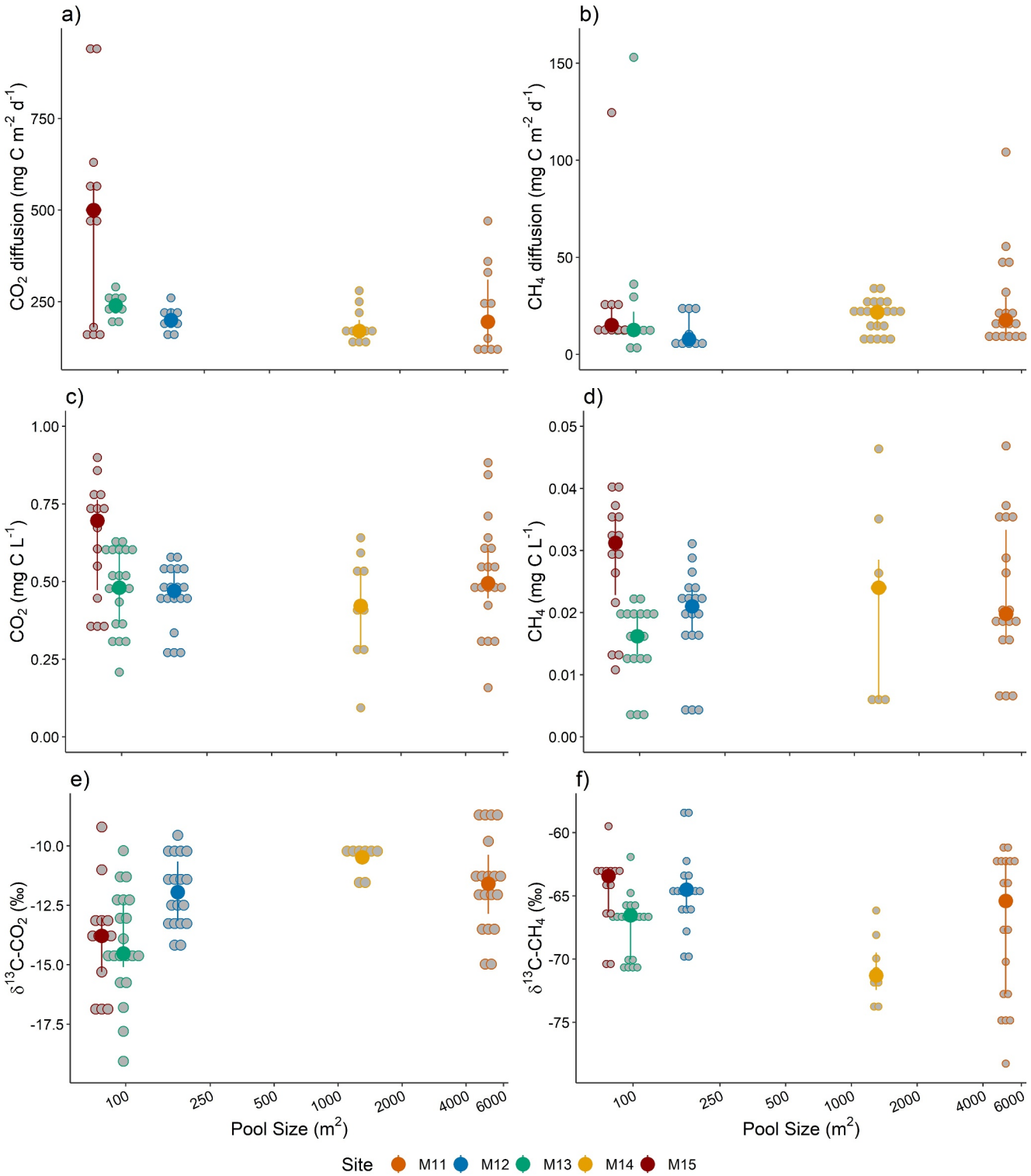

Figure 2. Diffusion fluxes (top panels a and b), surface water concentrations (middle panels c and d) and stable isotope ratios (bottom panels e and f) of CO_2 (a, c, and e) and CH_4 (b, d, and f) in the five studied pools presented by their surface area from smallest to largest, left to right. The gray dots show individual measurements. Larger colored dots represent the median value for each pool, with the vertical lines showing the interquartile ranges (25%–75% percentiles). Note that outliers were removed in each of the panels b (448, 299, and 298 mg C m^{-2} d^{-1}at M15; 188 and 173 mg C m^{-2} d^{-1} at M11) and d (1.1 μg C L^{-1} at M14, 1.0 μg C L^{-1} at M11, 0.7 μg C L^{-1} at M12, 0.1 μg C L^{-1} at M13).

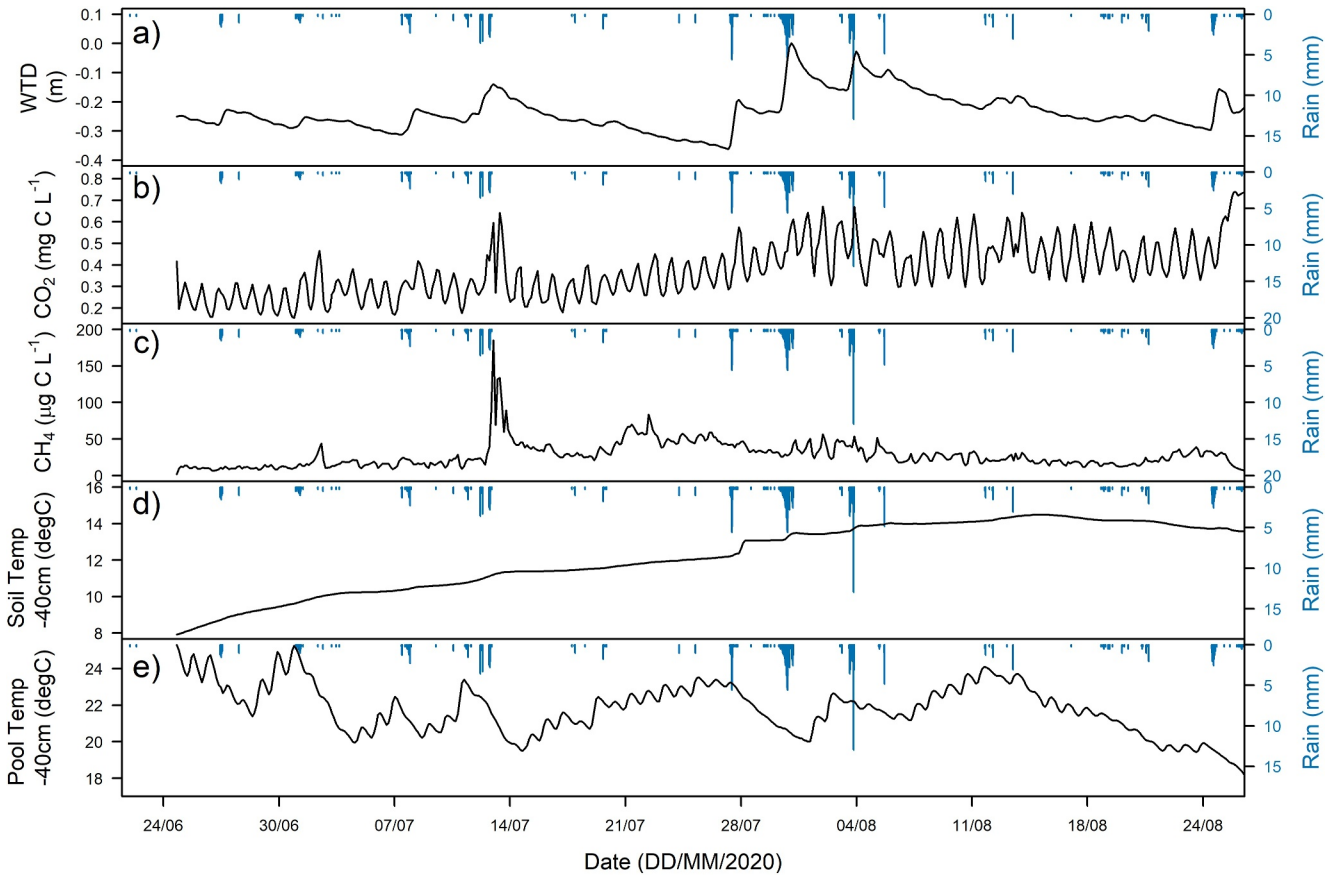

Figure 3. Continuous measurements in pool M11 from 25 June to 27 August 2020, of (a) peat water table depth (WTD), (b) dissolved CO_2 concentration, (c) dissolved CH_4 concentration, (d) soil (peat) temperature at −40 cm, and (e) pool temperature 40 cm below the water surface. Blue bars represent rainfall.

M15. Conversely, the lowest CO_2 concentrations and CO_2 fluxes were measured in M14, leaving the largest studied pool M11 aside (Figures 2a and 2e, and Table S2 in Supporting Information S1). The patterns of median isotopic values for CO_2 and CH_4 comparing the different pools mirrored each other (Figures 2i and 2j). On the contrary, the median $\delta^{13}C$-CO_2 in pools M11, M12, and M14 was lower compared to the smallest pool M15 (while it was slightly higher in M13; Figure 2e).

3.3. Variability of CO_2 and CH_4 Dynamics From Continuous Measurements

3.3.1. Temporal Variability Along the Growing Season

Over the 63 days of continuous measurements in pool M11 from 25 June to 27 August 2020, the median daily values (Q1–Q3) for CO_2 and CH_4 concentrations were 0.4 mg C L^{-1} (0.1–0.8 mg C L^{-1}) and 23.3 µg C L^{-1} (1.5–185.5 µg C L^{-1}), respectively (Figures 3b and 3c). The CO_2 concentrations increased over the growing season. All daily mean CO_2 concentrations above the seasonal median were measured after 26 July 2020, except for one earlier measurement on 13 July 2020 that coincided with a rain event (Figures 3a and 3b). Peat water table depth had a similar seasonal pattern as CO_2 concentrations, with 71% of the daily mean values above the seasonal median value (−0.25 m) being reported after 26 July 2020 (Figures 3a and 3b). The CH_4 concentrations followed a different seasonal trend, however. Most of the daily CH_4 concentrations above the seasonal median (24.0 µg C L^{-1}) were measured between 13 July and 11 August 2020, except for a few later CH_4 concentration measurements on 23–25 August, which also showed values above the median (Figure 3c). Peat temperature at −40 cm steadily increased throughout the growing season, starting at 11°C on 25 June and reaching a peak of 15.7°C on 19 August 2020 (Figure 3d). Pool water temperature was more consistent along the season, with a mean of 21.7°C. Pool water temperature increased over periods with no rain and decreased after a rain event (Figure 3e). Rain events did not seem to influence the CO_2 and CH_4 variability, except for 14 July 2020 when a clear increase

in CO_2 and CH_4 concentrations was observed following a four-day rain event (32 mm from 8 to 13 July 2020; Figures 3a–3c).

3.3.2. Diel Variability

Over the 63 days of continuous measurements in pool M11 from 25 June to 27 August 2020, we observed a clear pattern of higher CO_2 surface water concentration in the early morning at around 06:00, and lower in the early evening at around 19:00 (Figure 4a). The diel pattern of CH_4 surface water concentrations was not clear, however. We observed only slightly higher CH_4 surface water concentrations during daytime than during nighttime hours, where the median was highest between 06:00 and 13:00 (26.7 μg C L^{-1}), and lowest at 22:00 (19.3 μg C L^{-1}; Figure 4b). When plotted as a variation from the daily median, diel patterns are clearly visible for CO_2 (Figure 4c) but not for CH_4 (Figure 4d).

The discrete measurements in pools M11–M15 on 5–6 August 2019 revealed a pattern of most negative δ^{13}C-CO_2 (min: −21.4‰) in night hours (22:00–04:00), and least negative δ^{13}C-CO_2 (max: −7.2‰) in evening hours (16:00–18:00; Figure 4e). The δ^{13}C-CO_2 mirrored with the CO_2 surface water concentrations (Figures 4c and 4e). Neither δ^{13}C-CH_4 values nor CH_4 concentrations showed a comparable diel pattern (Figures 4d and 4f).

3.4. C-GHG Balance of the Pools

The overall mean CH_4 ebullition flux from all 16 deployed bubble traps was 7.5 mg C m^{-2} d^{-1}. Ebullitive CH_4 emission estimated from the 11 bubble traps deployed from 14 June to 7 August 2019 ranged from 0.6 to 6.2 mg C m^{-2} d^{-1} (median: 2.4 mg C m^{-2} d^{-1}; mean: 3.0 mg C m^{-2} d^{-1}). Between 7 August and 7 September 2019, CH_4 ebullition from five bubble traps ranged from 4.0 to 25.1 mg C m^{-2} d^{-1} (median: 20.4 mg C m^{-2} d^{-1}; mean: 17.4 mg C m^{-2} d^{-1}). As a rough estimate for the contribution of CH_4 ebullition to the overall peatland carbon budget, we multiplied this mean from the 16 traps by the total pool water surface area (108,112 m^2), resulting in an overall ebullitive emission of 813 kg C d^{-1} from the pools. The mean amount of CO_2 found in the captured bubbles by the 16 traps was 0.06 mg C m^{-2} d^{-1}, resulting in an overall contribution of 6 kg C d^{-1} from the total pool area.

Mean diffusive emission from the pools from 25 June to 27 August 2022 was 193.5 and 40.4 mg C m^{-2} d^{-1} for CO_2 and CH_4, respectively (Figure 5). Similar to what is reported in Section 3.3.1, a clear seasonal trend was observed, with greater C-GHG emissions toward the end of the time series, particularly for CO_2 but also a quick increase in emissions on 13 July 2020. The CO_2:CH_4 emission ratio fluctuated between 2.4 and 25.0, and the contribution of CH_4 to the total C-GHG release was the largest between 15 July and 31 July 2022. At the diel time scale, CO_2 emissions were on average 46% higher in the morning (i.e., before noon) than in the afternoon (Figure S1 in Supporting Information S1) and matched the CO_2 concentration diel variability (Figure 4c). The difference between morning and afternoon was only 7% for CH_4 diffusion. Summed up over the 64-day measurement period, a total of 15.0 g C m^{-2} was released from the pools, with CO_2 responsible for 83% of the total emissions (Figure 5).

3.5. Global Dataset of CO_2 and CH_4 Concentrations and Fluxes From Open-Water Peatland Pools

The dataset built from our systematic literature review includes 117 records of CO_2 concentration, 164 records of CH_4 concentration, 76 CO_2 flux values, 174 diffusion CH_4 flux values, and 63 ebullition CH_4 flux values from 283 unique sites and 38 independent publications (Supporting Information S2). All data were published between 1990 and 2023. Within this timeframe, 49% of the extracted data were published in 2020 or later. This suggests a growing scientific interest in peatland pools. Spatially, 54% of all sites are in Canada, followed by the European Union (20%), USA including Alaska (10%), Chile (9%), Russia (7%) and China (<1%). Concentrations and fluxes of CO_2 and CH_4 vary over several orders of magnitude (Figure S2 in Supporting Information S1). The average concentration is 1.43 mg C L^{-1} (median: 0.5 mg C L^{-1}) and 0.1 mg C L^{-1} (median: 0.0 mg C L^{-1}) for CO_2 and CH_4, respectively. The mean CO_2 diffusion flux is 1,039.0 mg C m^{-2} d^{-1} (median: 346.0 mg C m^{-2} d^{-1}), and the mean CH_4 diffusion flux is 53.0 mg C m^{-2} d^{-1} (median: 20.0 mg C m^{-2} d^{-1}). The mean CH_4 ebullition flux is 33.0 mg C m^{-2} d^{-1} (median: 8.0 mg C m^{-2} d^{-1}). The median CO_2 and CH_4 concentrations and fluxes from our study site were close to the global median values of other open-water peatland pools globally (Figure S2 in Supporting Information S1).

10.1029/2023GB007909

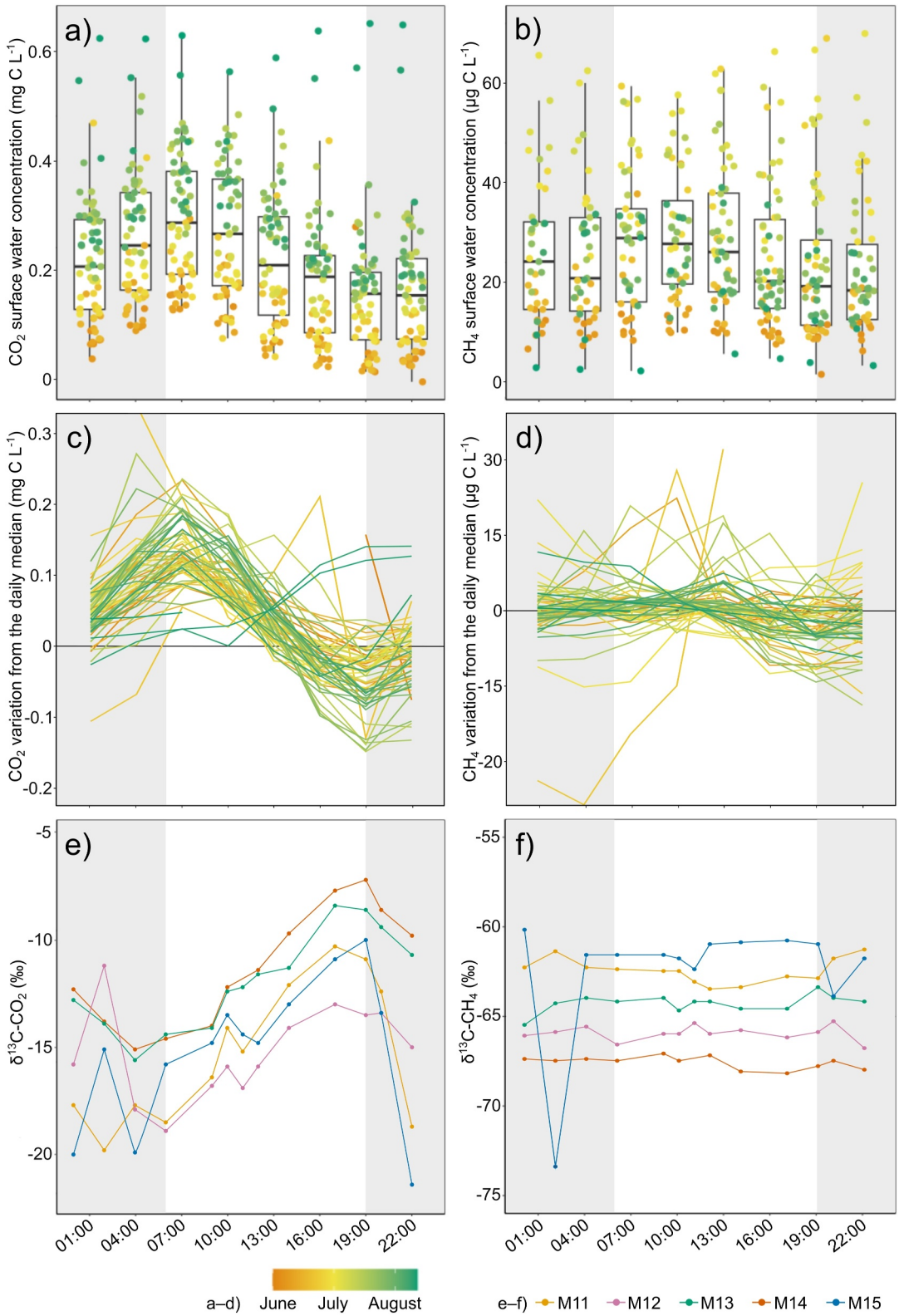

Figure 4.

4. Discussion

Open-water pools had considerably lower CO_2 and CH_4 concentrations than the adjacent peat porewater (Table S2 in Supporting Information S1), indicating that dissolved gas was transported from peat to pools and that substantial gas losses to the atmosphere occurred during this transport and from the pools. While the gradient in CO_2 and CH_4 concentration and stable isotope ratio between peat and water bodies (either streams or pools) have previously been observed (e.g., Campeau et al., 2018; Prijac et al., 2022; Rasilo et al., 2017), our study is the first to combine CO_2 and CH_4 stable isotope values and concentrations from open-water peatland pools, including a 64-day long continuous time series. This spatio-temporal dataset, along with a synthesis of the available data from the literature, allowed us to shed light on the importance of the dynamics in C-GHG processes between peat and pools and associate emissions with implications at the ecosystem and global scale.

4.1. Drivers of CO_2 and CH_4 Concentrations in the Peatland Pools

4.1.1. Predominant Contribution for Peat-Derived Organic Matter Degradation

Low δ^{13}C-CH_4 values such as those measured in the peat porewater of our studied system (-77.2 ± 3.6‰; Table S2 in Supporting Information S1) are typically reported from environments in which hydrogenotrophic methanogenesis (HM) is the main CH_4 source (Figure 6), including peatlands (Conrad, 2005; Galand et al., 2010; Holmes et al., 2015). In the studied pools' surface water, in contrast, δ^{13}C-CH_4 was higher (median: -64.3 ± 3.8‰). We explained the difference in CH_4 concentration and δ^{13}C-CH_4 between porewater and pool water by CH_4 oxidation (Figure 6), as observed and described by Zhang et al. (2016). Therefore, our CH_4 concentration gradient and δ^{13}C-CH_4 values support the hypothesis that CH_4 is produced in the peat and that some of it is transferred, either laterally or vertically, to the pools.

Unlike CH_4, dissolved CO_2 in the pools of our studied system originated from multiple potential sources, as the difference in median δ^{13}C-CO_2 between peat porewater (-3.8‰) and pool water (-12.4‰; Table S2 in Supporting Information S1) suggests. The first potential process is, as mentioned above, peat porewater input. The extremely high δ^{13}C-CO_2 in the peat porewater is explained by intense HM, which typically selects lighter CO_2 isotopes and generates high residual δ^{13}C-CO_2 (Okumura et al., 2016). Methanogenesis results in Rayleigh-type distillation (Whiticar, 1999), which, unlike autotrophic (i.e., root) and heterotrophic bacterial respiration, is a non-linear process. Therefore, the importance of methanogenesis explains the weak linear relationship observed in the Keeling plots (Figure S3 in Supporting Information S1) and the Miller-Tans plots (Figure 7b) for peat porewater. The Miller-Tans relationships were stronger for each of the five pools ($r^2 \geq 0.60$; Figure 7a) as compared to the peat porewater ($r^2 = 0.57$; Figure 7b), suggesting that organic matter decomposition from heterotrophic bacteria in pools was more important than in peat porewater. Nevertheless, the Miller-Tans relationships observed in pools were still weak compared to other sites where autotrophic and heterotrophic decomposition were identified as the exclusive sources of CO_2 (e.g., $r^2 = 0.99$ in Campeau et al. (2018)). The slopes of the linear Miller-Tans relationships, which can be used to identify the end-member (e.g., Campeau et al., 2018; Dean et al., 2023), were relatively consistent between the five pools (between -18.2‰ and -9.0‰; Figure 7a) and fell in between the δ^{13}C-CO_2 values expected from HM (-3.8‰ based on the porewater values) and ecosystem respiration (-30‰ to -25‰; Campeau, Bishop, et al., 2017; Campeau, Wallin, et al., 2017; Hutchins et al., 2020). Organic matter decomposition via heterotrophic activity in the pools was further supported by our diel analyses, where we measured greater CO_2 concentrations and lower δ^{13}C-CO_2 at night than at daytime (Figures 4a, 4c, and 4e). This diel pattern from both CO_2 concentration and δ^{13}C-CO_2 has been observed in other aquatic systems where in situ metabolism, predominated by heterotrophic respiration over autotrophic productivity, plays an active role as a net source of CO_2 into the system rather than a net sink (Rocher-Ros et al., 2021; Taillardat et al., 2022). As initially proposed, photochemical oxidation could also have played a role in explaining the CO_2 dynamics in the pools. However, Prijac et al. (2022) have previously concluded based on an in situ incubation experiment that such a

Figure 4. Panels (a)–(d) show three-hourly measurements of CO_2 and CH_4 surface water concentrations in pool M11 from 25 June to 27 August 2020: (a) CO_2 and (b) CH_4 grouped by hour of the day, and (c) CO_2 and (d) CH_4 presented by variation from the daily median, where the daily median was subtracted from the hourly measured value. Data in panels (a)–(d) are plotted on a continuous color scale along the season from June (orange) through July (yellow) to August (green). The bottom two panels (e)–(f) show diel measurements of (e) δ^{13}C-CO_2 and (f) δ^{13}C-CH_4 in the five open-water pools (M11–M15) on 5–6 August 2019. The gray background in all panels indicates nighttime.

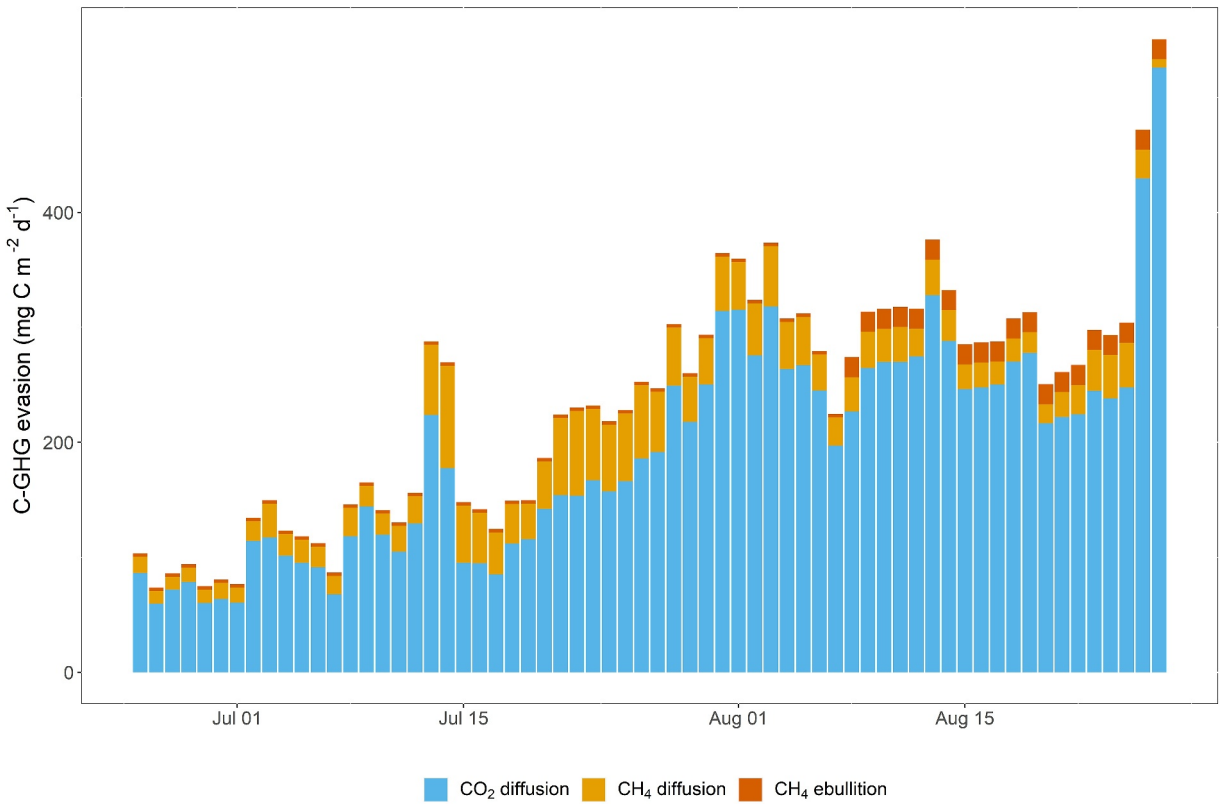

Figure 5. Time series of C-GHG evasion rate in mg C m^{-2} d^{-1} in pool M11 from 25 June to 27 August 2020, based on continuous measurements.

process was negligible at our study site. Similarly, CH_4 oxidation also contributed little to explaining CO_2 concentration in pools. Using a mass balance model based on one end-member (i.e., here, peat porewater) and in situ CH_4 concentrations and on $\delta^{13}C$-CH_4 values from Thottathil et al. (2018), we found that CH_4 oxidation contributed between 3.9% and 10.3% of the total CO_2 present in the pools (Table S3 in Supporting Information S1). This is a limited contribution that can be explained by low CH_4 concentration (20 times less) relative to CO_2 in the pools (Table S2 in Supporting Information S1).

Altogether, we conclude that the peatland pools at our study site have a consistent behavior among themselves (Figure 2). C-GHG concentrations and $\delta^{13}C$ values support the interpretation that most of the CH_4 and CO_2 present in the pools are the product of input from peat porewater, but that heterotrophic organic matter degradation within the pools also contributes to releasing CO_2 to a smaller extent. Other biogeochemical processes such as photooxidation and autotrophic microbial activity were also considered but did not appear to play a substantial role in our system. The diel CO_2 variation amplitude (Figures 3a and 3c) revealed that autotrophic microbial activity in the pools was at least twice lower than what was measured in the stream draining the peat (Figure S4 in Supporting Information S1), which was already considered to be a small component of the stream net carbon balance (Taillardat et al., 2022). The $\delta^{13}CO_2$ values and the slope of the Miller-Tans plot are further evidence suggesting that the lateral input from peat and heterotrophic bacteria activity played a larger role than CO_2 uptake from autotrophic bacteria.

4.1.2. Temporal Variability in C-GHG Dynamics

Our results suggest that water table level and temperature in peat and water are driving seasonal variability in CO_2 and CH_4 concentrations (Figure 3). Some previous studies highlighted the importance of temperature in explaining the concentration and flux variability in pools (McEnroe et al., 2009; Pelletier et al., 2014), while others did not observe any such significant relationship (Cliche Trudeau et al., 2013). The water table level seems to have influenced CO_2 concentrations, with greater pool CO_2 concentrations when the water table was low. A similar relationship has been reported for pools in a patterned fen (Cliche Trudeau et al., 2014), and also for the

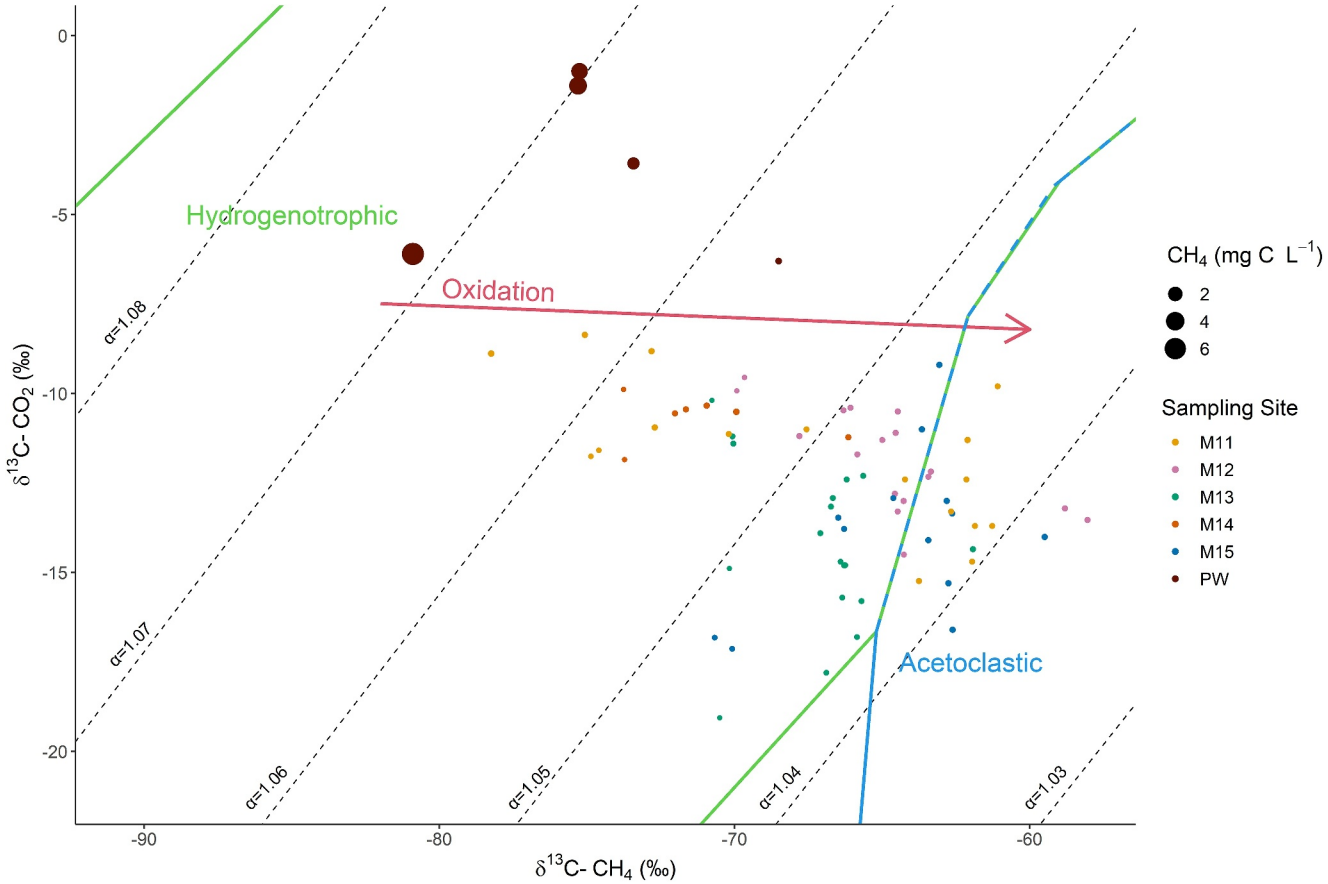

Figure 6. Crossplot of stable carbon isotope values in peat porewater (brown) and open-water pools (other colors). Dotted lines depict α-values. Note that the size of the dots is proportional to the CH_4 concentration. The oxidation line is from Knorr et al. (2009). The hydrogenotrophic and acetoclastic areas are from Negandhi et al. (2019). M11–M15 refer to surface water samples from the pools, and PW refers to peat porewater and well samples.

peat-draining stream of our study site (Taillardat et al., 2022). A probable explanation for this phenomenon is that a lower peat water table facilitates the lateral discharge of deeper and older peat porewater enriched in dissolved material (Covino, 2018). Water table level, however, does not appear to have influenced CH_4 concentrations in the pools (Figure 3). The inconsistent behavior of CO_2 and CH_4 may suggest that the peat-derived material follows different pathways: CO_2 and potentially oxidized CH_4 might predominantly be discharged to the pool from a lateral water movement, while CH_4 is principally produced at the bottom sediment of the pool (Campeau et al., 2021). Greater concentrations and fluxes occurred in the middle of the summer (Figure 3). Such a trend has been described previously and was explained by the warmer air, pool water, and surrounding peat temperatures over the summer, which stimulate both CO_2 and CH_4 production (McEnroe et al., 2009; Pelletier et al., 2014). Storms could have played a role in abruptly releasing large quantities of CO_2 and CH_4, as observed in large lakes (e.g., Vachon & del Giorgio, 2014). There was only one event (i.e., 13 July 2020) during our 64-day time series that might be linked to a storm release, but the emission magnitude remained within the same range as on the other days (Figure 5). Other than this, no dramatic changes from one day to the other linked with a rainfall event were reported. The fact that the pools are shallow, the peatland topography is flat, and surface runoff is limited as compared to porewater seepage (because of the high peat hydraulic conductivity) may indeed limit the effect of storms on C-GHG release from the peatland pools. At the diel scale, the majority of the CO_2 diffused in the morning with a peak of concentration and emission at ~7:00 a.m. (Figure 4a and Figure S1 in Supporting Information S1). These results contrast with the commonly reported nocturnal-versus-diurnal flux pattern explained primarily by the absence of CO_2 fixation by photosynthesis during nighttime (Attermeyer et al., 2021; Gómez-Gener et al., 2021). It is not clear to us why our results show a lag in maximum CO_2 emissions as compared to what has been reported, and it would require future investigations to determine if this observation is common for peatland pools and other aquatic ecosystems.

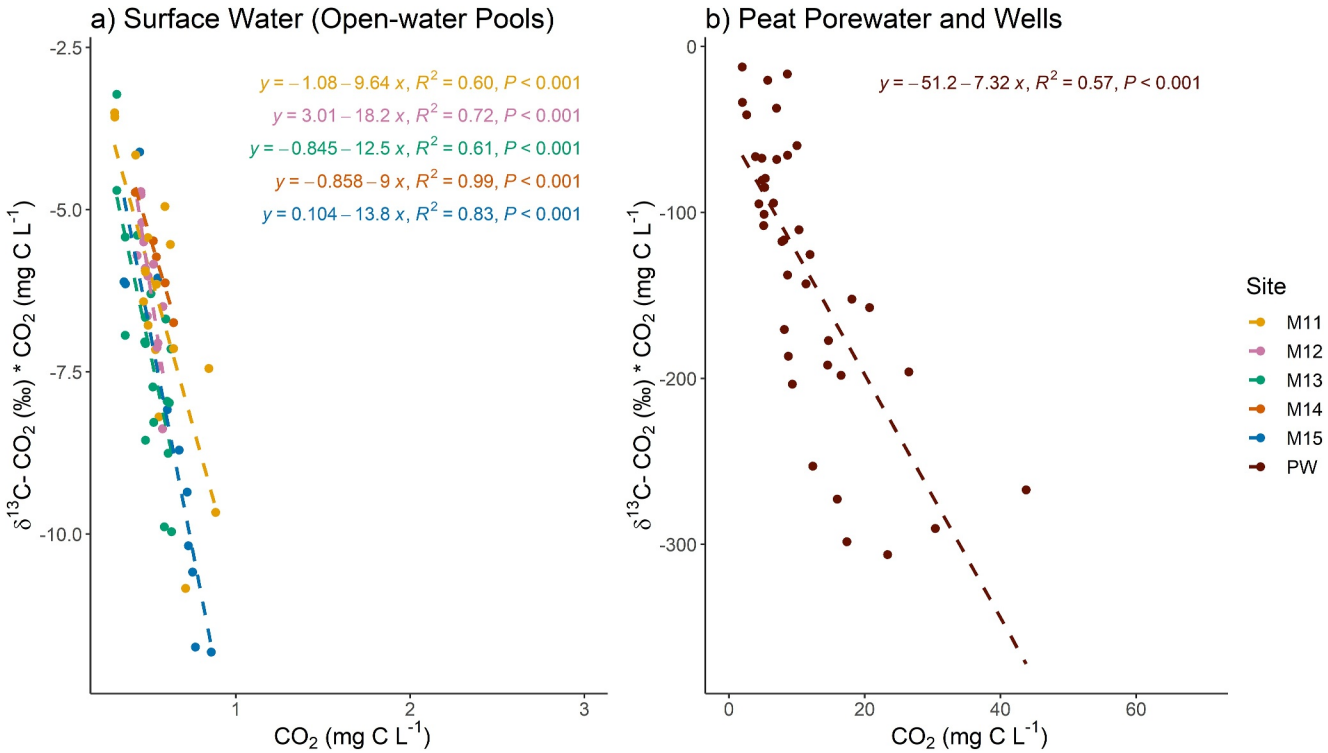

Figure 7. Miller-Tans plots showing $\delta^{13}C\text{-}CO_2$ * CO_2 vs. CO_2 concentration in (a) open-water pools M11–M15, and (b) peat porewater and wells (PW). The dashed color lines represent the linear regression models for each site.

4.1.3. Pool Size and Altimetry Seem to Influence the Spatial Variability in C-GHG Dynamics

The dimensions of the pools (Figure 2) together with seasonality (Figure 3) seem to have had the greatest impact on CO_2 and CH_4 concentrations and associated fluxes at our study site. If the largest pool M11 is taken out of the analysis, our dataset shows the greatest concentrations and fluxes from the smallest pools (Figure 2). For instance, pool M15 (surface of 77.2 m^2) had median CO_2 and CH_4 concentrations twice as large as M14 (1,298 m^2). Previous studies have established a relationship between pool dimensions (size and depth) with CO_2 and CH_4 concentrations and emissions at the site scale (Cliche Trudeau et al., 2013; McEnroe et al., 2009; Pelletier et al., 2014). The rationale is that, in general, smaller and shallower pools warm up faster, including the bottom sediment, which is thought to produce and release CO_2 and CH_4 (Pelletier et al., 2014). Although our dataset supports most of this argumentation, we noticed that the largest yet not deepest pool, M11 (5,085 m^2), did not fit into this relationship. M11 contained high CO_2 and CH_4 concentrations and generated strong fluxes closer to what was measured in the smallest pool M15 (Figure 2). One possible explanation is that because pool M11 is located at lower elevation than the other pools (Table S2 in Supporting Information S1), its drainage catchment might be larger, which would lead to greater quantities of carbon input.

The positive relationships between pool size and C-GHG concentrations and fluxes were also statistically significant at the global scale, according to our literature review (Figure 8). The CO_2 and CH_4 concentrations and the CH_4 diffusion and ebullition in our study were greatest in small pools and decreased with increasing pool size (Figures 8a, 8b, 8e, and 8f), which is similar to what was reported by Holgerson and Raymond (2016) for all types of lentic systems. However, unlike Holgerson and Raymond (2016), we found no significant positive linear relationships of CO_2:CH_4 ratio or CO_2 diffusion with water body size for peatland pools (Figures 8c and 8d). This may be because, regardless of their size, peatland pools are consistently surrounded by water-saturated and carbon-dense peat soils. This contrasts with the global dataset, which uses water body size as a proxy to lateral organic matter input, with greater perimeter-to-volume ratios and frequent mixing in smaller ponds (Holgerson & Raymond, 2016). Regarding the absence of a relationship between CO_2 diffusion and pool size (Figure 8d), larger pools may have a greater k_{600} because they are more exposed to wind and therefore gas diffusion, which compensates for the proportionally lower dissolved CO_2 concentration in smaller pools. However, we were unable to

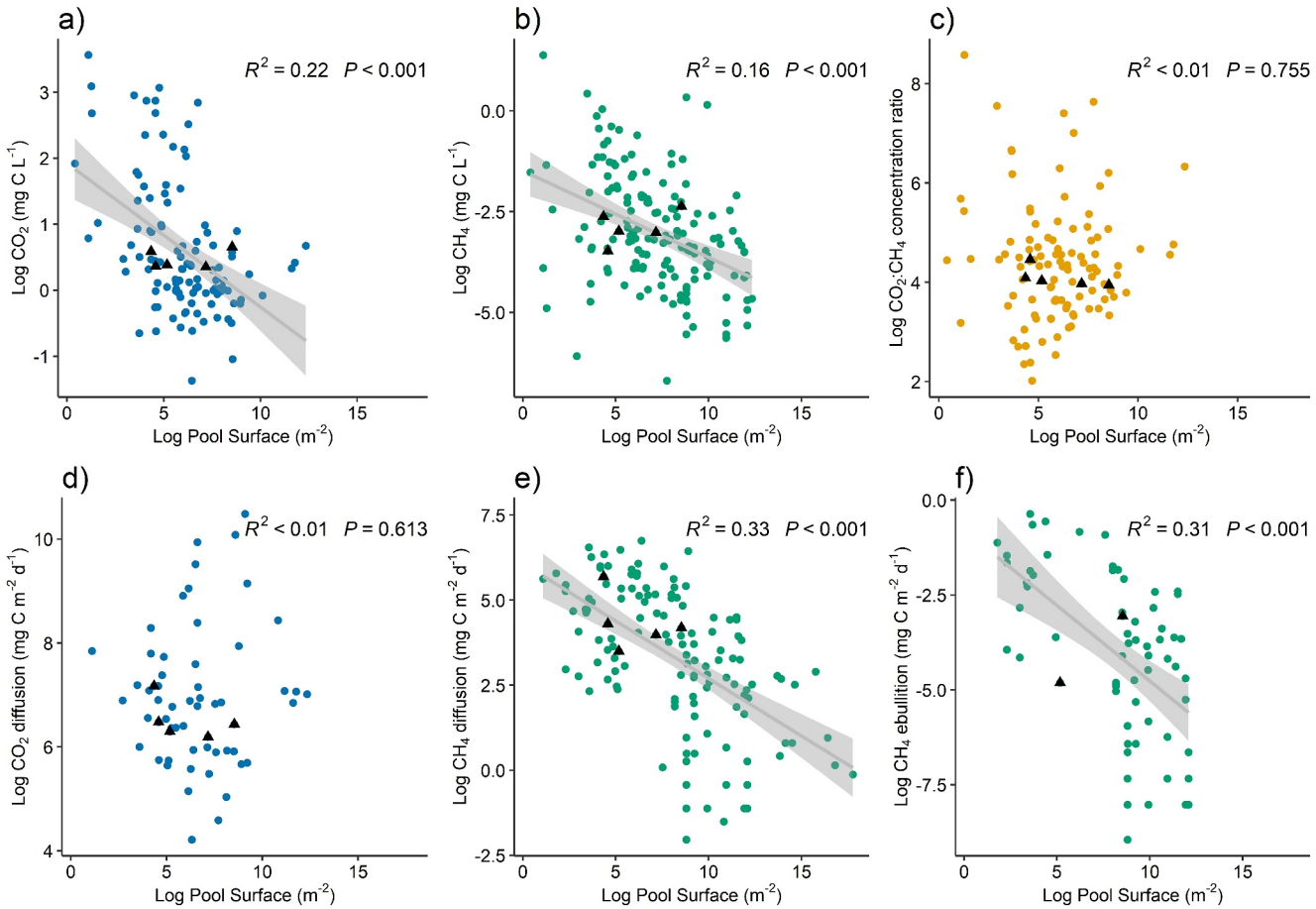

Figure 8. Linear relationships between peatland pool surface area and (a) CO_2 concentration, (b) CH_4 concentration, (c) CO_2:CH_4 concentration ratio, (d) CO_2 diffusion, (e) CH_4 diffusion, and (f) CH_4 ebullition. All axes are log-transformed on a natural log scale. The black triangles represent data from this study. The other data points are from previously published studies as compiled in our systematic literature review (Supporting Information S2).

establish a relationship between k_{600} and pool size, both at the study site and on a global scale. This is explained by the high spatiotemporal variability of k_{600} within and between sites, and the limited data available. For instance, only one study (i.e., Jansen et al., 2020) within our global dataset provided k_{600} values—which were nonetheless in good agreement with our average estimate of 0.95 m d^{-1} and 1.30 m d^{-1} for k_{600}-CO_2 and k_{600}-CH_4, respectively.

4.2. Biogeochemical Characteristics of Open-Water Peatland Pools Compared to Other Lentic Systems

Because of their small water surfaces and depths and their specific catchment properties, it is worth considering peatland pools as a distinct lentic freshwater system category (Richardson et al., 2022). However, our field study and literature review suggest that CO_2 or CH_4 emissions from open-water peatland pools are within the same range as those from other ponds, lakes, or reservoirs (Figure 9), despite their specific ecological properties.

Our literature review on open-water peatland pools (including results from this study) along with the dataset from Holgerson and Raymond (2016) from small ponds and thermokarst water bodies (both limited to <0.1 km^2 in this analysis for comparability) allowed us to compare dissolved CO_2, CH_4 concentration between these three different lentic systems (Figures 9a and 9b). Peatland pools had median CO_2 and CH_4 concentrations within the same range as small pools (less than 15% difference) at around 0.42 mg C L^{-1} and 15.40 µg C L^{-1}, respectively, while concentrations for both dissolved CO_2 and CH_4 in thermokarst were much more variable (Figures 9a and 9b). These results suggest that peatland pools and small ponds behave similarly as a consequence of their high perimeter-to-surface ratio and the proportionally important organic matter input compared to large lentic systems such as lakes and reservoirs. It is therefore probable that there are more ecological and biogeochemical similarities

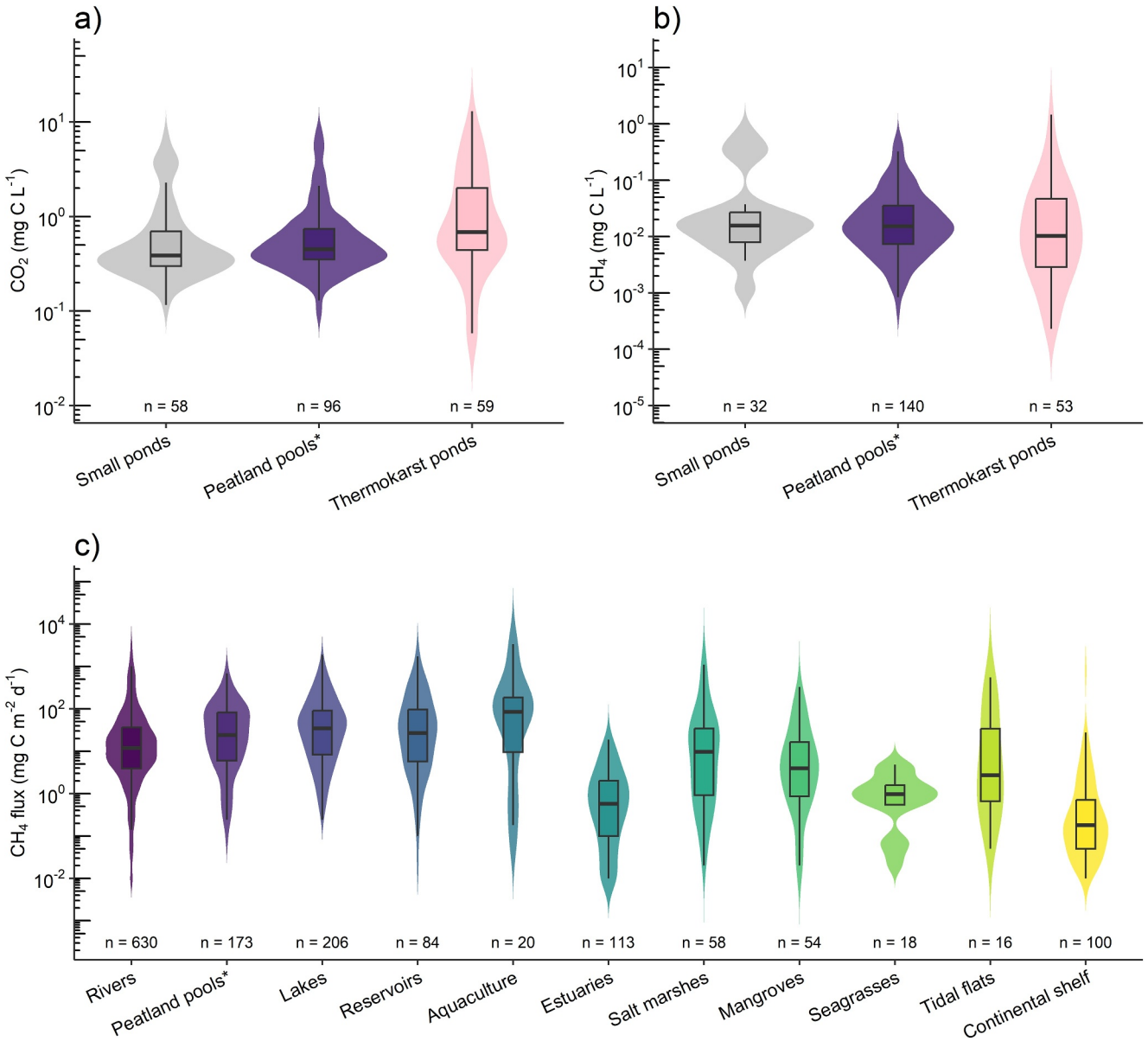

Figure 9. Comparison of (a) CO_2 concentrations, (b) CH_4 concentrations, and (c) CH_4 diffusion between peatland pools and other aquatic systems. Data for "Peatland pools*" in all three panels (a)–(c) are from this study. Data for "Small Ponds" and "Thermokarst Ponds" in panels (a) and (b) are from Holgerson and Raymond (2016), where only non-peat ponds <0.1 km^2 were kept. Data for the methane flux in panel (c), except for those from the "Peatland pools*", are from Rosentreter et al. (2021). All violin plots include box plots showing median, lower (Q1) and upper (Q3) quartiles, and 1.5 times the length of the interquartile range. The *y* axes of all panels (a)–(c) are log-transformed on a natural log (ln).

between small non-peat ponds (<0.1 km^2) and peatland pools than between small ponds and lakes in general. The substantially different median values and distributions of dissolved CO_2 and CH_4 concentrations in thermokarst (Figure 9a) can be explained by the vast group of systems they include (Kokelj & Jorgenson, 2013). Hence, thermokarst waterbodies would deserve a better categorization based on their size, depth, age and surrounding land cover (e.g., mineral, organic-rich permafrost, yedoma) to better understand their functioning and constrain their biogeochemical role (Arsenault et al., 2022; Dean et al., 2020; Kokelj & Jorgenson, 2013). This task is critical since thermokarst water bodies represent a substantial area of the Arctic region that is expected to increase as the climate gets warmer (Olefeldt et al., 2021).

Peatland pools at our study site released on average 278.7 (median: 220.0) mg C m^{-2} d^{-1} and 36.3 (median: 17.7) mg C m^{-2} d^{-1}, which is less than the average flux compiled from our global synthesis: 1,039.8 (median: 346.7)

mg C m^{-2} d^{-1} and 52.8 (median: 19.83) mg C m^{-2} d^{-1}. Similar to what we reported for dissolved C-GHG concentrations, peatland pools—including our study site—do not seem to generate higher CO_2 or CH_4 emissions when compared to water bodies of similar size. Global average emissions from small ponds (<0.1 km^2), which include some peatland pools, are 303 mg CO_2-C m^{-2} d^{-1} (range: 255–422 mg CO_2-C m^{-2} d^{-1} depending on the pond size categories) and 11.6 mg CH_4-C m^{-2} d^{-1} (3.36–27.48 mg CH_4-C m^{-2} d^{-1}; Holgerson & Raymond, 2016). We suggest that the large resources of degradable organic matter available in our peatland pools enhance dissolved C-GHG concentrations and emissions, but that this situation is not exclusive to peatland pools but rather common for small water bodies (<0.1 km^2) in general. Consequently, CH_4 emissions from peatland pools fall within the same range as other freshwater ecosystems (Figure 9c and Rosentreter et al., 2021) but do not represent a unique category based on the magnitude of their CH_4 or CO_2 release.

4.3. The Importance of Open-Water Peatland Pool C-GHG Emissions at the Ecosystem Scale

We acknowledge that our CO_2 and CH_4 budget estimates are likely to be underestimated since no emissions were accounted for during winter and spring snowmelt—seasons that have been described to have the potential to generate between 11% and 55% of the CO_2 and CH_4 in boreal and arctic lakes, including peatland pools (Karlsson et al., 2013; Lundin et al., 2013; Pelletier et al., 2014; Phelps et al., 1998; Riera et al., 1999). Two previous syntheses stressed the importance of aquatic carbon fluxes in net ecosystem carbon budgets and proposed an average offset between 20% and 40% for peat-dominated catchments, despite large variability between study sites and years (Taillardat et al., 2020; Webb et al., 2019). For instance, Leach et al. (2016) reported that in the peatland-dominated catchment during a dry year, stream carbon export alone offsets between 63% and 90% of the net ecosystem exchange (NEE = ER − GPP). According to Dean et al. (2023), most of the carbon released from peatland pools is from recent carbon primary production (<300 years old) rather than old carbon for deep peat layers (except perhaps for CH_4 ebullition), which confirms the need to integrate pool C-GHG exchange in annual peatland ecosystem carbon budgets.

At our study site, about 119,180 m^2 or 4.9% of the studied catchment area is composed of aquatic systems. Open-water pools dominate, accounting for 108,112 m^2 or 91% of the total aquatic area, whereas the stream accounts for 11,068 m^2 or the remaining 9% of the total aquatic area (Table S4 in Supporting Information S1). The mean concentrations in the pools were 7.9 and 1.4 times smaller than what was measured in the stream surface water for CO_2 and CH_4, respectively (Taillardat et al., 2022). Similarly, the CO_2 and CH_4 diffusion from the water to the atmosphere was about 35 (CO_2) and 2 (CH_4) times smaller for the pools than for the stream. The elevated C-GHG fluxes from the stream, in comparison to the pools, can be attributed to both the higher gas concentrations and the greater gas transfer velocities from the peat-draining turbulent stream, particularly for CO_2 (Crawford et al., 2014; Lundin et al., 2013). However, when their respective contribution is normalized to the catchment scale, CO_2 diffusion from the stream was only 3.6 times greater than that released by the pools, and CH_4 diffusion from pools was 4.6 times greater than that from the stream (Figure 10). This is because of the disproportional surface that pools occupy as compared to the stream (Table S4 in Supporting Information S1).

Similar observations were reported from two boreal catchments in Sweden (Jonsson et al., 2007; Lundin et al., 2013). While no NEE value is presently available for our study site, a literature review integrating the NEE from 13 northern ombrotrophic peatlands suggests an average carbon dioxide of −53.66 g C m^{-2} y^{-1} (Table S5 in Supporting Information S1), which is not substantially different from the long-term rate of carbon accumulation (LORCA) of 35.5 g C m^{-2} yr^{-1} for our study site (Primeau & Garneau, 2021). When using this literature-derived NEE value as the theoretical NEE at our study site (and normalized to the catchment surface), aquatic systems offset 22% of the carbon uptake, and open-water pools alone account for 4% of the offset (Figure 10). Our estimate is higher than that of Jonsson et al. (2007) who estimated that aquatic carbon losses offset 6% of the catchment NEE. However, Jonsson et al. (2007) mentioned that intensive forestry happening in the catchments might have artificially boosted the catchment's NEE. On the contrary, other studies reported a greater offset from pool C-GHG emissions between 39% and 45% in a restored ombrotrophic peatland in British Columbia (D'Acunha et al., 2019) or in northern permafrost wetlands (Kuhn et al., 2018). We conclude that the carbon outgassed and exported downstream from aquatic systems (i.e., pools and streams) in peat-dominated catchments represents a substantial, yet variable, loss from the peat-dominated catchment that needs to be accounted for to avoid overestimating the carbon capture and storage of peatlands (Casas-Ruiz et al., 2023).

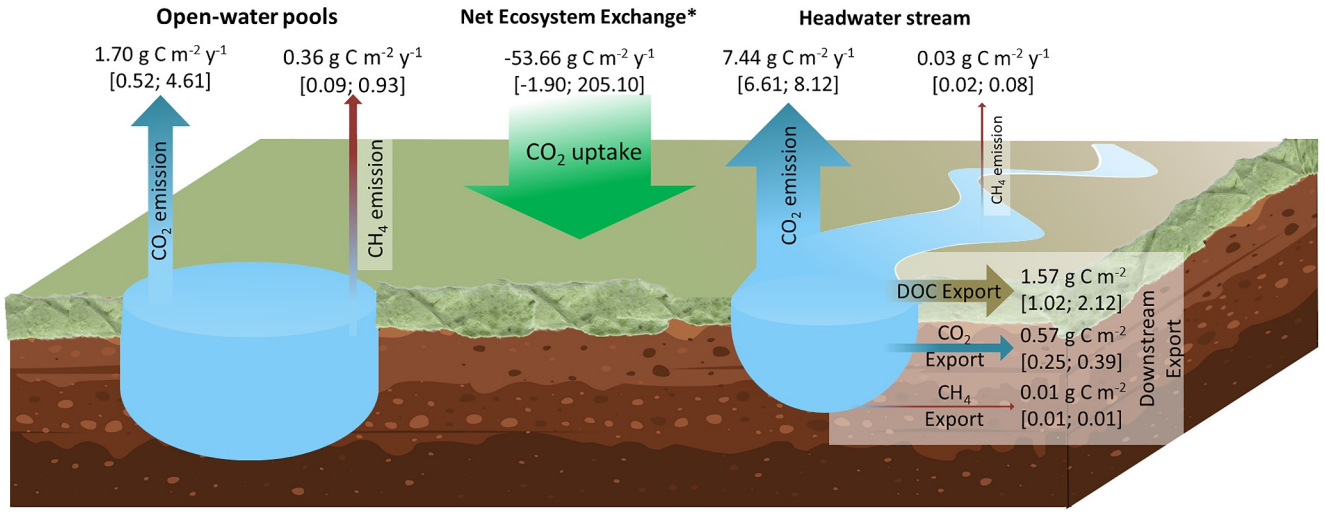

Figure 10. Conceptual model summarizing the studied net peatland-dominated catchment carbon balance. Data from open-water pools are from this study. Headwater stream CO_2 and CH_4 exchange and downstream export values are from Taillardat et al. (2022), headwater stream DOC downstream export values are from Prijac et al. (2023), and net ecosystem exchange (NEE) is from a synthesis of 13 previously published references that used eddy covariance measurements (see Table S5 in Supporting Information S1). Values in the conceptual model are normalized to the catchment surface by considering the respective surface of each land cover (i.e., terrestrial vegetation, open-water pools, and headwater stream). Annual emissions from the aquatic systems were calculated over 180 days, which was assumed to be the duration of the snow-free period in the region (Teodoru et al., 2009). Negative values indicate carbon uptake and values in brackets give the range.

5. Conclusion

This study highlights the biogeochemical importance of water bodies, including open-water pools, in the C-GHG balance of northern peatlands. The combination of spatial (five studied pools) and temporal (continuous 64-day time series in one pool) concentrations and fluxes of CO_2 and CH_4 allowed us to identify the origins and processes associated with carbon dynamics and emissions in open-water peatland pools, as well as estimate their carbon budget. The use of stable carbon isotopes helped identify methanogenesis-driven peat porewater input as the main source of dissolved CO_2 and CH_4 in peatland pools and that, to a smaller extent, heterotrophic bacterial in situ degradation also contributed to the release of CO_2 while autotrophic activity may have fixed a small fraction of the available CO_2. The automatic continuous time series of dissolved CO_2 and CH_4 concentrations allowed us to understand changes on an hourly basis such as the effect of autotrophic and heterotrophic activity; and on a monthly basis such as the effect of decreasing water table level and warming peat temperature on CO_2 and CH_4 concentration increase in pools, respectively. In addition, the spatial analysis from our study site along with the global dataset from our literature review showed that the pool size was a key variable to explain differences in dissolved CO_2 and CH_4 concentrations between pools. When compared to other aquatic systems, the gas concentrations and fluxes of open-water peatland pools at our site were within the expected range, which led us to conclude that even though open-water peatland pools are an ecologically distinct lentic system, their biogeochemical functioning and C-GHG exchange rates are close to what has previously been reported for small ponds (<0.1 km^2). However, it is very important to account for C-GHG emissions from water bodies within a peatland catchment to determine the net carbon balance since aquatic systems represent net carbon sources while the surrounding peat vegetation is typically characterized as a net carbon sink. Acknowledging the ecological and biogeochemical heterogeneity of peatlands is essential to truly assess their carbon removal potential at both the ecosystem and global scale.

Conflict of Interest

The authors declare no conflicts of interest.

Data Availability Statement

Datasets and metadata are available in the international research data repository Zenodo Taillardat (2024) [https://doi.org/10.5281/zenodo.10686116].

Acknowledgments
This research was funded by the Natural Sciences and Engineering Research Council of Canada and Hydro-Quebec to Michelle Garneau (RDCPJ 514218-17). We would like to thank Paul A. Del Giorgio for giving access to GRIL-UQAM laboratory facilities; Katherine Velghe for laboratory training and assistance; Charles Bonneau, Pénélope Germain-Chartrand, Charles-Élie Dubé-Poirier, Camille Girard, Léonie Perrier, Guillaume Primeau, Roman Teisserenc, and Karelle Trottier for their assistance in the field; Joshua Dean for his advice on thermokarst versus peatland pools distinction; the two reviewers Audrey Campeau and Gerard Rocher-Ros and the editors for their constructive comments and valuable advice during the peer-review process.

References

Arsenault, J., Talbot, J., Brown, L. E., Holden, J., Martinez-Cruz, K., Sepulveda-Jauregui, A., et al. (2022). Biogeochemical distinctiveness of Peatland Ponds, Thermokarst Waterbodies, and Lakes. *Geophysical Research Letters*, *49*(11), e2021GL097492. https://doi.org/10.1029/2021gl097492

Attermeyer, K., Casas-Ruiz, J. P., Fuss, T., Pastor, A., Cauvy-Fraunié, S., Sheath, D., et al. (2021). Carbon dioxide fluxes increase from day to night across European streams. *Communications Earth & Environment*, *2*(1), 1–8. https://doi.org/10.1038/s43247-021-00192-w

Bastviken, D., Tranvik, L. J., Downing, J. A., Crill, P. M., & Enrich-Prast, A. (2011). Freshwater methane emissions offset the continental carbon sink. *Science*, *331*(6013), 50. https://doi.org/10.1126/science.1196808

Battin, T. J., Lauerwald, R., Bernhardt, E. S., Bertuzzo, E., Gómez-Gener, L., Hall, R. O., et al. (2023). River ecosystem metabolism and carbon biogeochemistry in a changing world. *Nature*, *613*(7944), 449–459. https://doi.org/10.1038/s41586-022-05500-8

Belyea, L. R., & Lancaster, J. (2002). Inferring landscape dynamics of bog pools from scaling relationships and spatial patterns. *Journal of Ecology*, *90*(2), 223–234. https://doi.org/10.1046/j.1365-2745.2001.00647.x

Butman, D., Stackpoole, S., Stets, E., McDonald, C. P., Clow, D. W., & Striegl, R. G. (2016). Aquatic carbon cycling in the conterminous United States and implications for terrestrial carbon accounting. *Proceedings of the National Academy of Sciences of the United States of America*, *113*(1), 58–63. https://doi.org/10.1073/pnas.1512651112

Campeau, A., Bishop, K., Nilsson, M. B., Klemedtsson, L., Laudon, H., Leith, F. I., et al. (2018). Stable carbon isotopes reveal soil-stream DIC linkages in contrasting headwater catchments. *Journal of Geophysical Research: Biogeosciences*, *123*(1), 149–167. https://doi.org/10.1002/2017JG004083

Campeau, A., Bishop, K. H., Billett, M. F., Garnett, M. H., Laudon, H., Leach, J. A., et al. (2017). Aquatic export of young dissolved and gaseous carbon from a pristine boreal fen: Implications for peat carbon stock stability. *Global Change Biology*, *23*(12), 5523–5536. https://doi.org/10.1111/gcb.13815

Campeau, A., Vachon, D., Bishop, K., Nilsson, M. B., & Wallin, M. B. (2021). Autumn destabilization of deep porewater CO_2 store in a northern peatland driven by turbulent diffusion. *Nature Communications*, *12*(1), 1–13. https://doi.org/10.1038/s41467-021-27059-0

Campeau, A., Wallin, M. B., Giesler, R., Löfgren, S., Mörth, C. M., Schiff, S., et al. (2017). Multiple sources and sinks of dissolved inorganic carbon across Swedish streams, refocusing the lens of stable C isotopes. *Scientific Reports*, *7*(1), 1–14. https://doi.org/10.1038/s41598-017-09049-9

Casas-Ruiz, J. P., Bodmer, P., Bona, K. A., Butman, D., Couturier, M., Emilson, E. J. S., et al. (2023). Integrating terrestrial and aquatic ecosystems to constrain estimates of land-atmosphere carbon exchange. *Nature Communications*, *14*(1), 1571. https://doi.org/10.1038/s41467-023-37232-2

Cliche Trudeau, N., Garneau, M., & Pelletier, L. (2013). Methane fluxes from a patterned fen of the northeastern part of the La Grande river watershed, James Bay, Canada. *Biogeochemistry*, *113*(1–3), 409–422. https://doi.org/10.1007/s10533-012-9767-3

Cliche Trudeau, N., Garneau, M., & Pelletier, L. (2014). Interannual variability in the CO_2 balance of a boreal patterned fen, James Bay, Canada. *Biogeochemistry*, *118*(1–3), 371–387. https://doi.org/10.1007/s10533-013-9939-9

Comas, X., Slater, L., & Reeve, A. S. (2011). Pool patterning in a northern peatland: Geophysical evidence for the role of postglacial landforms (Vol. *399*, pp. 173–184). https://doi.org/10.1016/j.jhydrol.2010.12.031

Conrad, R. (2005). Quantification of methanogenic pathways using stable carbon isotopic signatures: A review and a proposal. *Organic Geochemistry*, *36*(5), 739–752. https://doi.org/10.1016/j.orggeochem.2004.09.006

Core Team, R. (2021). A language and environment for statistical computing. Retrieved from https://www.r-project.org/

Covino, T. (2018). Hydrologic connectivity as a framework for understanding biogeochemical flux through watersheds and along fluvial networks Geomorphology Hydrologic connectivity as a framework for understanding biogeochemical fl ux through watersheds and along fluvial ne, (September 2016). https://doi.org/10.1016/j.geomorph.2016.09.030

Crawford, J. T., Lottig, N. R., Stanley, E. H., Walker, J. F., Hanson, P. C., Finlay, J. C., & Striegl, R. G. (2014). CO_2 and CH_4 emissions from streams in a lake-rich landscape: Patterns, controls, and regional significance. *Global Biogeochemical Cycles*, *28*(3), 197–210. https://doi.org/10.1111/1462-2920.13280

D′Acunha, B., Morillas, L., Black, T. A., Christen, A., & Johnson, M. S. (2019). Net ecosystem carbon balance of a peat bog undergoing restoration: Integrating CO_2 and CH_4 fluxes from eddy covariance and aquatic evasion with DOC drainage fluxes. *Journal of Geophysical Research: Biogeosciences*, *124*(4), 884–901. https://doi.org/10.1029/2019JG005123

Dean, J. F., Billett, M. F., Turner, T. E., Garnett, M. H., Andersen, R., Mckenzie, R. M., et al. (2023). Peatland pools are tightly coupled to the contemporary carbon cycle, (July) (pp. 1–16). https://doi.org/10.1111/gcb.16999

Dean, J. F., Meisel, O. H., Martyn Rosco, M., Marchesini, L. B., Garnett, M. H., Lenderink, H., et al. (2020). East Siberian Arctic inland waters emit mostly contemporary carbon. *Nature Communications*, *11*(1), 1627. https://doi.org/10.1038/s41467-020-15511-6

Deblois, C. P., Demarty, M., Bilodeau, F., & Tremblay, A. (2023). Automated CO_2 and CH_4 monitoring system for continuous estimation of degassing related to hydropower, (June) (pp. 1–12). https://doi.org/10.3389/fenvs.2023.1194994

Dickson, A. G. (1990). Standard potential of the reaction: $AgCl(s) + 1\ 2H_2(g) = Ag(s) + HCl(aq)$, and the standard acidity constant of the ion HSO_4^- in synthetic sea water from 273.15 to 318.15 K. *The Journal of Chemical Thermodynamics*, *22*(2), 113–127. https://doi.org/10.1016/0021-9614(90)90074-Z

Environment Canada. (2023). Past weather and climate historical data. Retrieved from https://climate.weather.gc.ca/historical_data/search_historic_data_e.html

Foster, D. R., King, G. A., Glaser, P. H., & Wright, H. E. (1983). Origin of string patterns in boreal peatlands. *Nature*, *306*(5940), 256–258. https://doi.org/10.1038/306256a0

Frankignoulle, M., Abril, G., Borges, A., Bourge, I., Canon, C., Delille, B., et al. (1998). Carbon dioxide emission from European estuaries. *Science*, *282*(5388), 434–436. https://doi.org/10.1126/science.282.5388.434

Galand, P. E., Yrjälä, K., & Conrad, R. (2010). Stable carbon isotope fractionation during methanogenesis in three boreal peatland ecosystems. *Biogeosciences*, *7*(11), 3893–3900. https://doi.org/10.5194/bg-7-3893-2010

Garneau, M., Tremblay, L., & Magnan, G. (2018). Holocene pool formation in oligotrophic fens from boreal Québec in northeastern Canada. *The Holocene*, *28*(3), 396–407. https://doi.org/10.1177/0959683617729439

Goldenfum, J. A. (2011). GHG measurement guidelines for freshwater reservoirs.

Golub, M., Koupaei-Abyazani, N., Vesala, T., Mammarella, I., Ojala, A., Bohrer, G., et al. (2023). Diel, seasonal, and inter-annual variation in carbon dioxide effluxes from lakes and reservoirs. *Environmental Research Letters*, *18*(3), 034046. https://doi.org/10.1088/1748-9326/acb834

Gómez-Gener, L., Rocher-Ros, G., Battin, T., Cohen, M. J., Dalmagro, H. J., Dinsmore, K. J., et al. (2021). By high nocturnal emissions. *Nature Geoscience*, *14*(5), 289–294. https://doi.org/10.1038/s41561-021-00722-3

Granéli, W., Lindell, M., De Faria, B. M., & Esteves, F. D. A. (1998). Photoproduction of dissolved inorganic carbon in temperate and tropical lakes - Dependence on wavelength band and dissolved organic carbon concentration. *Biogeochemistry*, *43*(2), 175–195. https://doi.org/10.1023/A:1006042629565

Hanson, R. S., & Hanson, T. (1996). Methanotorphic Bacteria. *Microbiological Reviews*, *60*(2), 439471. https://doi.org/10.1128/mr.60.2.439-471.1996

Harris, L. I., Roulet, N. T., & Moore, T. R. (2019). Mechanisms for the development of microform patterns in Peatlands of the Hudson Bay Lowland. *Ecosystems*, *23*(4), 741–767. https://doi.org/10.1007/s10021-019-00436-z

Holgerson, M. A., & Raymond, P. A. (2016). Large contribution to inland water CO_2 and CH_4 emissions from very small ponds. *Nature Geoscience*, *9*(3), 222–226. https://doi.org/10.1038/ngeo2654

Holmes, M. E., Chanton, J. P., Tfaily, M. M., & Orgam, A. (2015). CO_2 and CH_4 isotope compositions and production pathways in a tropical peatland. *Global Biogeochemical Cycles*, *29*, 1–18. https://doi.org/10.1111/1462-2920.13280

Hutchins, R. H. S., Tank, S. E., Olefeldt, D., Quinton, W. L., Spence, C., Dion, N., et al. (2020). Fluvial CO_2 and CH_4 patterns across wildfire-disturbed ecozones of subarctic Canada: Current status and implications for future change. *Global Change Biology*, *26*(4), 2304–2319. https://doi.org/10.1111/gcb.14960

Jansen, J., F. Thornton, B., Cortés, A., Snöälv, J., Wik, M., MacIntyre, S., & Crill, P. M. (2020). Drivers of diffusive CH_4 emissions from shallow subarctic lakes on daily to multi-year timescales. *Biogeosciences*, *17*(7), 1911–1932. https://doi.org/10.5194/bg-17-1911-2020

Jonsson, A., Algesten, G., Bergström, A. K., Bishop, K., Sobek, S., Tranvik, L. J., & Jansson, M. (2007). Integrating aquatic carbon fluxes in a boreal catchment carbon budget. *Journal of Hydrology*, *334*(1–2), 141–150. https://doi.org/10.1016/j.jhydrol.2006.10.003

Karlsson, J., Giesler, R., Persson, J., & Lundin, E. (2013). High emission of carbon dioxide and methane during ice thaw in high latitude lakes. *Geophysical Research Letters*, *40*(6), 1123–1127. https://doi.org/10.1002/grl.50152

Knorr, K. H., Lischeid, G., & Blodau, C. (2009). Dynamics of redox processes in a minerotrophic fen exposed to a water table manipulation. *Geoderma*, *153*(3–4), 379–392. https://doi.org/10.1016/j.geoderma.2009.08.023

Kokelj, S. V., & Jorgenson, M. T. (2013). Advances in thermokarst research. *Permafrost and Periglacial Processes*, *24*(2), 108–119. https://doi.org/10.1002/ppp.1779

Kuhn, M., Lundin, E. J., Giesler, R., Johansson, M., & Karlsson, J. (2018). Emissions from thaw ponds largely offset the carbon sink of northern permafrost wetlands. *Scientific Reports*, *8*(1), 1–7. https://doi.org/10.1038/s41598-018-27770-x

Kumar, M., Yadav, A. N., Saxena, R., Rai, P. K., Paul, D., & Tomar, R. S. (2021). Novel methanotrophic and methanogenic bacterial communities from diverse ecosystems and their impact on environment. *Biocatalysis and Agricultural Biotechnology*, *33*, 102005. https://doi.org/10.1016/j.bcab.2021.102005

Leach, J. A., Larsson, A., Wallin, M. B., Nilsson, M. B., & Laudon, H. (2016). Twelve year interannual and seasonal variability of stream carbon export from a boreal peatland catchment. *Journal of Geophysical Research: Biogeosciences*, *121*(7), 1851–1866. https://doi.org/10.1002/2016JG003357

Lewis, E., Wallace, D., & Allison, L. J. (1998). Program developed for CO_2 system calculations: Carbon Dioxide. *Information Analysis Center*. https://doi.org/10.2172/639712

Lide, D. R. (2007). *Handbook of chemistry and physics* (88th ed.). CRC Press.

Lundin, E. J., Giesler, R., Persson, A., Thompson, M. S., & Karlsson, J. (2013). Integrating carbon emissions from lakes and streams in a subarctic catchment. *Journal of Geophysical Research: Biogeosciences*, *118*(3), 1200–1207. https://doi.org/10.1002/jgrg.20092

McEnroe, N. A., Roulet, N. T., Moore, T. R., & Garneau, M. (2009). Do pool surface area and depth control CO_2 and CH_4 fluxes from an ombrotrophic raised bog, James Bay, Canada? *Journal of Geophysical Research*, *114*(1), 1–9. https://doi.org/10.1029/2007JG000639

Millero, F. J., Graham, T. B., Huang, F., Bustos-Serrano, H., & Pierrot, D. (2006). Dissociation constants of carbonic acid in seawater as a function of salinity and temperature. *Marine Chemistry*, *100*(1–2), 80–94. https://doi.org/10.1016/j.marchem.2005.12.001

Negandhi, K., Edwards, G., Kelleway, J. J., Howard, D., Safari, D., & Saintilan, N. (2019). Blue carbon potential of coastal wetland restoration varies with inundation and rainfall. *Scientific Reports*, *9*(1), 1–9. https://doi.org/10.1038/s41598-019-40763-8

Okumura, T., Kawagucci, S., Saito, Y., Matsui, Y., Takai, K., & Imachi, H. (2016). Hydrogen and carbon isotope systematics in hydrogenotrophic methanogenesis under H2-limited and H2-enriched conditions: Implications for the origin of methane and its isotopic diagnosis. *Progress in Earth and Planetary Science*, *3*(1), 2–15. https://doi.org/10.1186/s40645-016-0088-3

Olefeldt, D., Hovemyr, M., Kuhn, M. A., Bastviken, D., Bohn, T. J., Connolly, J., et al. (2021). The boreal-arctic wetland and lake dataset (BAWLD). *Earth System Science Data*, *13*(11), 5127–5149. https://doi.org/10.5194/essd-13-5127-2021

Payette, S., Fortin, M. J., & Gamache, I. (2001). The subarctic forest-tundra: The structure of a biome in a changing landscape. *BioScience*, *51*(9), 709–718. https://doi.org/10.1641/0006-3568(2001)051%5B0709,TSFTTS%5D2.0.CO;2

Pelletier, L., Strachan, I. B., Garneau, M., & Roulet, N. T. (2014). Carbon release from boreal peatland open water pools: Implication for the contemporary C exchange. *Journal of Geophysical Research: Biogeosciences*, *119*(3), 2292–2311. https://doi.org/10.1002/2013JG002423. Received

Phelps, A. R., Peterson, K. M., & Jeffries, O. (1998). Methane efflux from high-latitude lakes during spring ice melt. *Journal of Geophysical Research*, *103*(D22), 29029–29036. https://doi.org/10.1029/98jd00044

Prijac, A., Gandois, L., Jeanneau, L., Taillardat, P., & Garneau, M. (2022). Discontinuity of the concentration and composition of dissolved organic matter at the peat-pool interface in a boreal peatland. *Biogeosciences*, *19*(18), 4571–4588. https://doi.org/10.5194/bg-19-4571-2022

Prijac, A., Gandois, L., Taillardat, P., Bourgault, M. A., Riahi, K., Ponçot, A., et al. (2023). Hydrological connectivity controls dissolved organic carbon exports in a peatland-dominated boreal catchment stream. *Hydrology and Earth System Sciences*, *27*(21), 3935–3955. https://doi.org/10.5194/hess-27-3935-2023

Primeau, G., & Garneau, M. (2021). Carbon accumulation in peatlands along a boreal to subarctic transect in eastern Canada. *The Holocene*, *31*(1), 1–12. https://doi.org/10.1177/0959683620988031

Rasilo, T., Hutchins, R. H. S., Ruiz-González, C., & del Giorgio, P. A. (2017). Transport and transformation of soil-derived CO_2, CH_4 and DOC sustain CO_2 supersaturation in small boreal streams. *Science of the Total Environment*, *579*, 902–912. https://doi.org/10.1016/j.scitotenv.2016.10.187

Raymond, P. A., Hartmann, J., Lauerwald, R., Sobek, S., McDonald, C., Hoover, M., et al. (2013). Global carbon dioxide emissions from inland waters. *Nature*, *503*(7476), 355–359. https://doi.org/10.1038/nature12760

Raymond, P. A., Saiers, J. E., & Sobczak, W. V. (2016). Hydrological and biogeochemical controls on watershed dissolved organic matter transport: Pulse-shunt concept. *Ecology*, *97*(1), 5–16. https://doi.org/10.1890/14-1684.1

Regnier, P., Resplandy, L., Najjar, R. G., & Ciais, P. (2022). The land-to-ocean loops of the global carbon cycle. *Nature*, *603*(7901), 401–410. https://doi.org/10.1038/s41586-021-04339-9

Reis, P. C. J., Thottathil, S. D., & Prairie, Y. T. (2022). The role of methanotrophy in the microbial carbon metabolism of temperate lakes. *Nature Communications*, *13*(1), 1–9. https://doi.org/10.1038/s41467-021-27718-2

Richardson, D. C., Holgerson, M. A., Farragher, M. J., Hoffman, K. K., King, K. B. S., Alfonso, M. B., et al. (2022). A functional definition to distinguish ponds from lakes and wetlands. *Scientific Reports*, *12*(1), 1–13. https://doi.org/10.1038/s41598-022-14569-0

Riera, J. L., Schindler, J. E., & Kratz, T. K. (1999). Seasonal dynamics of carbon dioxide and methane in two clear-water lakes and two bog lakes in northern Wisconsin, U.S.A. *Canadian Journal of Fisheries and Aquatic Sciences*, *56*(2), 265–274. https://doi.org/10.1139/f98-182

Rocher-Ros, G., Harms, T. K., Sponseller, R. A., Väisänen, M., Mörth, C. M., & Giesler, R. (2021). Metabolism overrides photo-oxidation in CO_2 dynamics of Arctic permafrost streams. *Limnology & Oceanography*, *66*(S1), S169–S181. https://doi.org/10.1002/lno.11564

Rocher-ros, G., Stanley, E. H., Loken, L. C., Casson, N. J., Raymond, P. A., Liu, S., et al. (2023). Global methane emissions from rivers and streams. *Nature*, *621*(7979), 530–535. https://doi.org/10.1038/s41586-023-06344-6

Rosentreter, J. A., Borges, A. V., Deemer, B. R., Holgerson, M. A., Liu, S., Song, C., et al. (2021). Half of global methane emissions come from highly variable aquatic ecosystem sources. *Nature Geoscience*, *14*(4), 225–230. https://doi.org/10.1038/s41561-021-00715-2

Sand-Jensen, K., Riis, T., Kjær, J. E., & Martinsen, K. T. (2022). Stream-lake connectivity is an important control of fluvial CO_2 concentrations and emissions in catchments. *Earth and Space Science*, *9*(12), e2022EA002664. https://doi.org/10.1029/2022EA002664

Schubert, C. J., Vazquez, F., Lösekann-Behrens, T., Knittel, K., Tonolla, M., & Boetius, A. (2011). Evidence for anaerobic oxidation of methane in sediments of a freshwater system (Lago di Cadagno). *FEMS Microbiology Ecology*, *76*(1), 26–38. https://doi.org/10.1111/j.1574-6941.2010.01036.x

Sivan, O., Adler, M., Pearson, A., Gelman, F., Bar-Or, I., John, S. G., & Eckert, W. (2011). Geochemical evidence for iron-mediated anaerobic oxidation of methane. *Limnology & Oceanography*, *56*(4), 1536–1544. https://doi.org/10.4319/lo.2011.56.4.1536

Taillardat, P. (2024). A carbon source in a carbon sink: Carbon dioxide and methane dynamics in open-water peatland pools (Version 3) [Dataset]. *Zenodo*. https://doi.org/10.5281/zenodo.10686116

Taillardat, P., Bodmer, P., Deblois, C. P., Ponçot, A., Prijac, A., Riahi, K., et al. (2022). Carbon dioxide and methane dynamics in a peatland headwater stream: Origins, processes and implications. *Journal of Geophysical Research: Biogeosciences*, *127*(7), 1–27. https://doi.org/10.1029/2022JG006855

Taillardat, P., Thompson, B. S., Garneau, M., Trottier, K., & Friess, D. A. (2020). Climate change mitigation potential of wetlands and the cost-effectiveness of their restoration. *Interface Focus*, *10*(5), 20190129. https://doi.org/10.1098/rsfs.2019.0129

Teodoru, C. R., Del Giorgio, P. A., Prairie, Y. T., & Camire, M. (2009). Patterns in pCO_2 in boreal streams and rivers of northern Quebec, Canada. *Global Biogeochemical Cycles*, *23*(2), 1–11. https://doi.org/10.1029/2008GB003404

Thottathil, S. D., Reis, P. C. J., del Giorgio, P. A., & Prairie, Y. T. (2018). The extent and regulation of summer methane oxidation in northern lakes. *Journal of Geophysical Research: Biogeosciences*, *123*(10), 3216–3230. https://doi.org/10.1029/2018JG004464

Vachon, D., & del Giorgio, P. A. (2014). Whole-lake CO_2 dynamics in response to storm events in two morphologically different lakes. *Ecosystems*, *17*(8), 1338–1353. https://doi.org/10.1007/s10021-014-9799-8

Wanninkhof, R. (1992). Relationship between wind speed and gas exchange over the ocean. *Journal of Geophysical Research*, *97*(C5), 7373–7382. https://doi.org/10.1029/92JC00188

Webb, J. R., Santos, I. R., Maher, D. T., & Finlay, K. (2019). The importance of aquatic carbon fluxes in net ecosystem carbon budgets: A catchment-scale review. *Ecosystems*, *22*(3), 508–527. https://doi.org/10.1007/s10021-018-0284-7

Weiss, R. F. (1974). Carbon dioxide in water and seawater: The solubility of a non-ideal gas. *Marine Chemistry*, *2*(3), 203–215. https://doi.org/10.1016/0304-4203(74)90015-2

Whiticar, M. J. (1999). Carbon and hydrogen isotope systematics of bacterial formation and oxidation of methane. *Chemical Geology*, *161*(1), 291–314. https://doi.org/10.1016/S0009-2541(99)00092-3

Zhang, G., Yu, H., Fan, X., Ma, J., & Xu, H. (2016). Carbon isotope fractionation reveals distinct process of CH4 emission from different compartments of paddy ecosystem. *Scientific Reports*, *6*, 1–10. https://doi.org/10.1038/srep27065